PhD Thesis

Classical and Quantum Behavior of Dipoles on a Helix

Jakob Knorborg Pedersen

Department of Physics and Astronomy

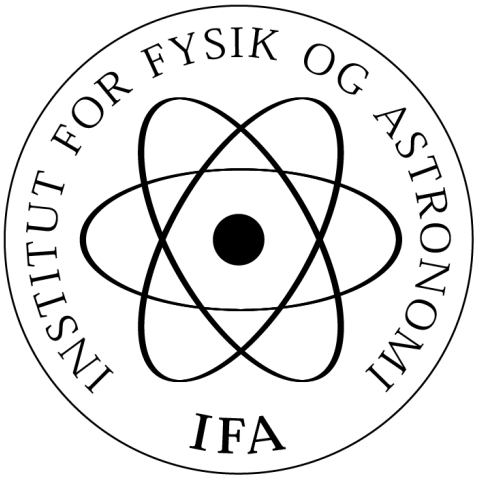

Aarhus University, Denmark

2015

Jakob Knorborg Pedersen
Department of Physics and Astronomy
Aarhus University
Ny Munkegade, Bldg. 1520
8000 Aarhus C
Denmark
E-mail: jkp07@phys.au.dk

This dissertation has been submitted to the Faculty of Science and Technology at Aarhus University, Denmark, in partial fulfillment of the requirements for the PhD degree in physics. The work presented has been performed in the period from May 2012 to November 2015 under the supervision of Aksel S. Jensen and Nikolaj T. Zinner. The work was carried out at the Department of Physics and Astronomy in Aarhus.

Contents

Contents v

Summary/Resumé vii
Summary . . . vii
Resumé . . . vii

Acknowledgements ix

List of publications xi

1 Introduction 1
1.1 Cold atoms . . . 2
1.2 The Dipole interaction . . . 2
1.3 Thesis outline . . . 3

2 The Helix 5
2.1 Introduction . . . 5
2.2 Dipoles On A Helix . . . 6

3 Classical Crystals 9
3.1 Classical Energy . . . 9
3.2 Normal modes and stability . . . 12
3.3 Stability . . . 14
3.4 Small systems . . . 16
3.5 Speed of sound . . . 18
3.6 Summary . . . 21

4 Numerical Methods 23
4.1 Grid based methods . . . 23
4.2 Integration based methods . . . 26

5 Quantum single-particle properties in a one-dimensional curved space 29
5.1 Classical Description . . . 29
5.2 Quantizing the motion . . . 30
5.3 Solutions in different geometries . . . 35
5.4 Summary . . . 47

6 Few-body states of dipoles on a helix 51
6.1 One dipole . . . 51
6.2 Two dipoles . . . 52

6.3 Three dipoles 56

7 Summary and Outlook **63**

Bibliography **67**

Summary/Resumé

Summary

This dissertation investigates the effects of confining dipoles in a helically shaped trap. First classical properties of dipoles trapped on a helix are investigated. The strong head-to-tail attraction between dipoles means that the dipoles form chains along the helix. The stability of these chain structures is investigated, how it depends on the total number of dipoles, and on the shape of the helix. After that, a discussion on how to develop a quantum mechanical description of a single particle trapped in an effectively one dimensional trap with varying curvature follows. This is done through two different approaches. One starting for a classical description in one dimension, and then from that developing a quantum mechanical description. The other approach starts from a quantum mechanical description in three dimensions, and the effects of the trap can then be approximated by an adiabatic expansion which results in an one dimensional description. The final part of the dissertation is about the quantum mechanical properties of a system of two or three dipoles trapped on a helix.

Resumé

Denne afhandling undersøger effekterne af at begrænse dipoler til en fælde formet som en helix. Til at starte med undersøges de klassiske egenskaber af dipoler fanget på en helix. Den stærke tiltrækning mellem dipoler betyder at dipolerne danner kæder langs helixen. Stabiliteten af disse strukturer af kæder undersøges, hvordan den afhænger af antallet af dipoler, samt hvordan den afhænger af helixens form. Derefter diskutteres det hvordan man kvantemekanisk kan beskrive en enkelt partikel fanget i hvad der effektivt er en endimensional fælde med varierende krumning. Dette gøres med to forskellige tilgange. én som starter fra en klassisk beskrivelse i én dimension, og fra den finde en kvantemekanisk beskrivelse. Den anden starter med en kvantemekanisk beskrivelse i tre dimensioner, hvor effekterne af fælden approksimeres med en adiabatisk ekspansion, hvilket resulterer i en endimensional beskrivelse. Den sidste del afhandlingen omhandler systemer af to eller tre dipoler fanget på en helix.

Acknowledgements

I would like to begin with thanking my two supervisors Aksel Jensen and Nikolaj Zinner. Their help and guidance throughout the last four years have been both inspirational and important for the completion of this project. In addition to having two supervisors I have also enjoyed the benefit of having Dmitri Fedorov in our group. I have received help from him with anything from technical computer issues to complex questions relating to the project. I would also like to thank all the other members of the sub-atomic group: Filipe Bellotti, Amin Dehkharghani, Hans Fynbo, Dennis Hove, Alan Howard, Oliver Kirsebom, Gunvor Koldste, Kasper Laursen, Morten Lund, Michael Munch, Jonas Refsgaard, Karsten Riisager, Artem Volosniev, Peder Sørensen, Jacob Johansen and Oleksandr Marchukov. The enthusiastic discussions over lunch, football tournaments and hockey games have been a privilege to be part of and have made the last years joyful. A special thank you to Oleksandr for his help with Latex issues during the final phase of the project. Finally, I would like to thank my girlfriend Lina for her patience and support. I might have to do the dishes for a very long time.

List of publications

This thesis is based on the following papers

- Jakob K Pedersen, Dmitri V. Fedorov, Aksel S. Jensen and Nikolaj T. Zinner: *Formation of classical crystals of dipolar particles in a helical geometry,* Journal of Physics B: At. Mol. Opt. Phys. **47 (2014) 165103**
- Jakob K Pedersen, Dmitri V. Fedorov, Aksel S. Jensen and Nikolaj T. Zinner: *Quantum single-particle properties in a one-dimensional curved space,* Accepted for publication in Journal of Modern Optics.
- Jakob K Pedersen, Dmitri V. Fedorov, Aksel S. Jensen and Nikolaj T. Zinner: *Quantum few-body bound states of dipolar particles in a helical geometry,* In review at Journal of Physics B: At. Mol. Opt. Phys.

Chapter 1

Introduction

The first systems we encounter when we study physics are one dimensional systems. From the free falling stone in classical mechanics to the particle in a box in quantum mechanics. But one dimensional systems, are not only interesting as a tool for teaching physics. They have unique properties that are not found in two and three dimensional systems. The unique physical properties of one dimensional systems reduces the numerical complexities in solving one dimensional systems. Several numerical techniques are applicable to one dimensional systems without having obvious ways to generalize them to higher dimensional systems

One of the ways that one dimensional systems differ from higher dimensional systems is that if the particles interact they cannot pass by one another, they have to pass through each other if possible and interact. This means that if we have an interaction between particles it always leads to collective behavior and it is not generally possible to describe the system through single particle states. Another difference is that the kinetic energy in one dimension does not have a centrifugal term. This means that any two body potential with a negative integral over the entire space leads to a bound state[1]. Because no phase transition can occur in one dimension, it is not possible even at zero temperature to have long range order. At zero temperature the order parameter follows a power law, but no true crystal structure is possible in one dimension.

One dimensional systems have been realized in several different ways. In quantum wires and in organic polymers, but it is in the field of cold atoms that some of the most promising one dimensional systems are found[2, 3, 4]. The control of both the geometry of the one dimensional system, and the interaction between the particles in it is what makes cold atoms such an interesting tool to study one dimensional physics. Typically cold atoms are trapped in effectively harmonic traps where ω_x, ω_y and ω_z denotes the trapping frequencies in all directions. By changing the trapping frequencies in such a manner that the trapping in two of the directions is much stronger than in the third, one can enter what is effectively a one dimensional system. The frequencies in the strong trapping direction are denoted $\omega_\perp$ and in the weak direction $\omega_\parallel$. One can enter an effectively one-dimensional system when the trapping in the orthogonal directions $\omega_\perp$ is so large that the spacing between the oscillator levels $\hbar\omega_\perp$ is much larger than the typical energies of the trapped particles[5]. This also means that if two trapped atoms form a strongly bound molecule then the energy released in such a reaction might be enough to take them out the one dimensional system.

1.1 Cold atoms

Since the work of Steven Chu in the 80's there have been much in improvement on the trapping and cooling of neutral atoms[6]. With the creation of a Bose Einstein condensate in the 90's [7] the field of cold atoms exploded. It is now possible to create condensates of several different atoms, and mix two different species in the same condensate[8]. Cold atom physics is a promising field with interesting prospects both in itself, and as a way to simulate other more complex quantum systems[9, 10]. A major reason for this is the ability to control the interaction between the atoms, and the geometry of the system.

The interaction between cold atoms is usually modeled by a contact interaction $g\delta(\mathbf{r})$, or more conveniently by the scattering length a, Through the relation $g = \frac{4\pi a\hbar}{m}$. It is this scattering length a that can be tuned through what is know as Feshbach resonances[11, 12]. A Feshbach resonance is a phenomenon where two different reaction channels have different magnetic moments, and changing an external magnetic field then changes the energy difference between the channels. When the energy of the interacting atoms matches that of the upper channel a resonant behavior is seen and the scattering length diverges. The occurrence of Feshbach resonances and their location is well studied for many atomic species, and through precise control of the external magnetic field, almost any value a a is attainable. This feature to tune the interaction between cold atoms is one of the things that make cold atoms system ideal if one wants to construct quantum simulators to study more complex solid state systems. By tuning the scattering length to be very large one can enter a universal regime where interesting things like the Efimov effect appears[13, 14]. Cold atomic gases do have losses and the number of particles is not constant. One of the ways for the atoms to fall out of the trap is if they form bound states that are deep enough so that the energy released by forming the bound state is enough throw them out of the trap. This effect have been used to study three body physics where the loss rate can be linked to the formation of three body bound states.

1.2 The Dipole interaction

The dipole-dipole interaction is interesting in the area of ultracold atoms, since it has some features that are very different from the van-der-Waals forces that typically are the dominant forces between ultracold atoms[15]. The dipole-dipole interaction is long rang and scales as $1/r^3$. But even more interesting is the fact that it is anisotropic. The strength and the sign of the interaction depends on the angle between the two dipoles. Two dipoles oriented head-to-tail attract and two polarized dipoles side by side repel each other. The long range and anisotropic nature of the dipole interaction means that it is not possible to map it onto a contact interaction of the form $g\delta(\mathbf{r})$, like one usually does for the van-der-Waals type interactions between cold atoms. Systems where the atoms only interact through dipole-dipole interactions are only found in textbooks. In principle the relevant parameter is the relative strength of the dipole interaction compared to the scattering length that is used to describe the interaction between cold atoms.

There are several ways of obtaining ultracold dipoles. They split into two distinct categories, magnetic and electric dipoles. For magnetic dipoles, the problem is that for the alkali atoms that are usually used for cold atom experiments, and the dipole moment

in the groundstate is only about one Bohr magneton. So to observe effects of the dipole interacting one would have to tune the interacting through Feshbach resonances such that the scattering length becomes small and dipole-dipole effects become comparable. Another choice is to find atoms with a higher magnetic moment one such atom is ^{52}Cr[16], which has a magnetic moment of $6\mu_B$, and from which a condensate has been made.

For electric dipoles there are a few different ways of displacing the charges in the atoms and obtaining electric dipoles. The first way is to form molecules [17, 18, 19, 20, 21, 22, 23, 24, 25]. For the molecules to have a permanent electric dipole moment they have to be heteronuclear. The ground state of molecules is the rotationally symmetric $J = 0$ state, so an external electric field is needed to orient the molecules in the laboratory frame. It is however very hard to cool molecules. One way to get around this problem is to start with an already cold two component gas and then tuning the interaction between the two species through Feshbach resonances to form heteronuclear molecules. The dipole moment of molecular dipoles is much higher than that of magnetic dipoles, and it possible to enter regimes where the dipole-dipole interaction is the dominant interaction.

Another way to obtain electric dipoles is through Rydberg atoms[26]. For Rydberg atoms the radius of the electron orbit scales as the square of the principle quantum number n. This means that the dipole moment scales as n^2. Individual Rydberg atoms have lifetimes that are long enough to do experiments with them. But because of the weak binding of the valence electrons and the strong interactions between Rydberg atoms the lifetimes of the atoms in dense gases is much shorter than for free atoms.

The head-to-tail attraction between dipoles makes a dipolar system unstable against losses in three dimensions. This leads to attempts to study such systems in lower dimensional setups such as trapping the dipoles in one or more layers of two dimensional pancakes[24]. If the dipoles within a pancake is aligned such that the interaction between two dipoles is attractive the system is unstable because of collapse. But if they are aligned in a way such the interaction is repulsive, the system is stable. This is the case for polarization perpendicular to the pancakes. If one stacks several of these pancakes on top of each other it is possible to form bound states between two dipoles in different layers[27, 28]. Another way to stabilize a gas of dipoles is to put it in an optical lattice. The long range nature of the dipole interaction leads to novel quantum phases, such as charge density waves and super solid phases[29].

1.3 Thesis outline

Chapter 2

In this chapter we define the helix and the coordinates used to describe the position of particles on a helix. We discuss different methods of creating helically shaped traps for neutral particles. Finally we discuss the dipole-dipole interaction, and how it looks between two dipoles confined to move along a helix.

Chapter 3

In this chapter we look at systems of several dipoles confined to move on a helix. We approach this from a classical point of view, and look at the crystal structures that appear when one traps a large number of dipoles on a helix.

Chapter 4

In this chapter we look at the numerical methods we are going to use when we solve the quantum mechanical problems in the following chapters.

Chapter 5

In this chapter we investigate the non-trivial problem of developing a quantum mechanical description of a one dimensional system with a varying curvature. We approach it from two directions. First from a classical description in one dimension and then quantizing this system. The varying curvature leads to a position dependent effective mass, and this leads to a non-trivial quantization step where there are several choices of operator ordering. Which choice is correct is not a priori known and we discuss two different ways of doing it. The second approach we use is starting from a fully quantized description is three dimensions, and then through an adiabatic approximation we reduce it to a one dimensional problem, but now with an extra potential term. We explore and compare these different approaches for three different perturbations on the helical geometry.

Chapter 6

Here we discuss the formation of two- and three-body bound states of dipoles trapped on a helix. We look at it for different experimentally relevant interaction strengths. We discuss the size and structure of the bound states of both two and three dipoles.

Chapter 7

Finally, we give a short summary of the thesis and discuss possible directions for future work in the field.

Chapter 2

The Helix

2.1 Introduction

Optical trapping of ultracold atoms provides the most promising way of obtaining a system of particles confined to a helix. There are two distinct approaches to this. One way of obtaining a helical trap is through the interference between Laguerre-Gaussian beams with nonzero angular momentum. The nonzero angular momentum refers to higher order Laguerre-Gaussian beams also known as "donut" modes, because of the shape of the intensity profile of the laser beam. An example of such a mode is shown in figure 2.1. One way to create these Laguerre-Gaussian beams is through holographic generation where a hologram is constructed in such a way that when it is illuminated with a regular Gaussian beam it produces a diffraction pattern of higher order LG-beams. The holograms can even be made such that most of the intensity goes into the desired order of Laguerre-Gaussian beam. Two counter propagating Laguerre-Gaussian beams can be used to generate a helically shaped trap [30]. The use of free propagating beams is limited by the Rayleigh length, which is the distance along the beam axis at which the cross sectional area of the beam doubles. This puts a limit on the maximum size of the helix, and on the minimum length at which the helix parameters can be modulated.

Another way of trapping ultracold atoms in helical geometry is to trap it in the

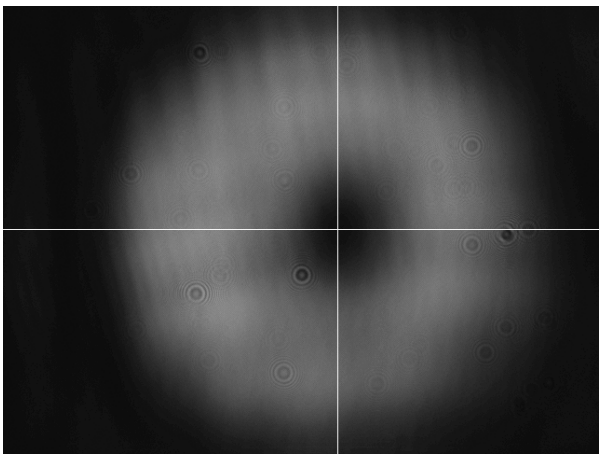

Figure 2.1: A cross section of a Laguerre-Gaussian beam with nonzero angular momentum. Notice the donut like shape of the intensity with a dark spot in the center and high intensity in a circle around it.

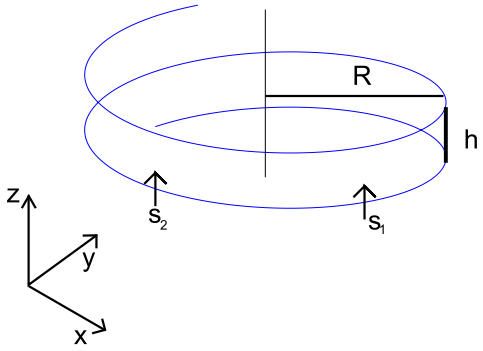

Figure 2.2: A schematic drawing of a helix with radius R and pitch h. In the bottom corner the Cartesian axes are shown. Two dipoles, s_1 and s_2, are shown with their dipole moments aligned with the symmetry axis.

evanescent field surrounding a tapered optical fiber [31]. When a laser field that is otherwise resonant with an optical fiber reaches a tapered region of the fiber it is no longer resonant and an evanescent field surrounding the fiber appears. It is this evanescent field that can be used to trap cold atoms. By choosing red or blue detuned beams one can create a helically shaped trap for cold atoms surrounding the fiber. This approach leads to a high degree of control of the different parameters of the helix.

2.2 Dipoles On A Helix

The helix is a curve that revolves around a fixed axis. It is described by two parameters, R and h. R is the radius at which the curve revolves around the axis, and h, called the pitch, is the vertical distance after one revolution around the axis. It is useful to parameterize the helix by the arc length measured along the helix s. Doing so a helix is parameterized in the following way

$$\{x, y, z\} = \left\{ R\sin\left(s/\alpha\right), R\cos\left(s/\alpha\right), \frac{hs}{2\pi\alpha} \right\}. \tag{2.1}$$

Where $\alpha = \sqrt{R^2 + \left(\frac{h}{2\pi}\right)^2}$. α is the relation between the arc length and the angle around the axis ϕ, such that $\phi = s/\alpha$. In figure 2.2 a sketch of a helix is shown. Helices appear in two distinct versions left hand and right handed versions, depending on which way they rotate. The one shown in figure 2.2 is left handed.

The Dipole-Dipole Interaction

With two or more dipoles on a helix, the long range interaction is given by the dipole-dipole interaction that is known for two dipoles in three dimensions. If the dipoles are located at $\boldsymbol{r}_i$ and $\boldsymbol{r}_j$ then the two dipole interaction is [32]

$$V(\boldsymbol{r}_i, \boldsymbol{r}_j) = \frac{1}{4\pi\epsilon_0}\frac{1}{r^3}\left[\boldsymbol{d}\cdot\boldsymbol{d} - 3\left(\boldsymbol{d}\cdot\hat{\boldsymbol{r}}\right)\left(\boldsymbol{d}\cdot\hat{\boldsymbol{r}}\right)\right], \tag{2.2}$$

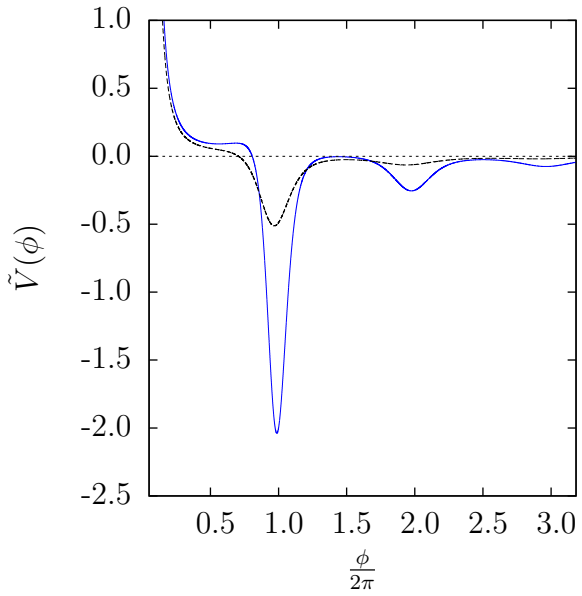

Figure 2.3: The reduced potential, $\tilde{V} = 4\pi R^3 \epsilon_0 V/d^2$, of two dipoles as a function of the relative angle, $\phi = \phi_i - \phi_j$, separating the particles on the helix. The helix parameters are chosen to be $h = R$ (blue solid) and $h = 1.6R$ (black dashed).

where $r = |\boldsymbol{r}_i - \boldsymbol{r}_j|$ is the distance between the dipoles and $\hat{\boldsymbol{r}} = (\boldsymbol{r}_i - \boldsymbol{r}_j)/r$ is the unit vector in the direction connecting the two dipoles. The unit used here is $\frac{1}{4\pi\epsilon_0}$, where ϵ_0 is the vacuum permittivity. This corresponds to a choice of electric dipoles, but nothing prevents this formalism from being used with magnetic dipoles if the unit is changed to $\frac{\mu_0}{4\pi}$, where μ_0 is the vacuum permeability. We assume the dipole moments of all the particles to be aligned along the z-axis by an external electric field (see figure 2.2). As mentioned earlier it is then more convenient to describe the position of the dipoles by their position along the helix rather than their Cartesian coordinates. This can be done through the transformation in equation 2.1. Denoting the position of the two dipoles along the helix by ϕ_i and ϕ_j, the two-dipole potential then becomes

$$V(\phi_i, \phi_j) = \frac{d^2}{4\pi\epsilon_0} \frac{2R^2\left[1 - \cos\left(\phi_i - \phi_j\right)\right] - 2h^2\left(\left(\phi_i - \phi_j\right)/(2\pi)\right)^2}{\left(2R^2\left[1 - \cos\left(\phi_i - \phi_j\right)\right] + h^2\left(\left(\phi_i - \phi_j\right)/(2\pi)\right)^2\right)^{5/2}}. \tag{2.3}$$

When the dipoles are aligned in the z-direction, then the interaction potential between two dipoles trapped on a helix only depends on the relative distance between the two dipoles $\phi = \phi_i - \phi_j$. The two-dipole potential is shown as a function of the dipole separation in figure 2.3. The long range part of the two-dipole potential falls of as ϕ^{-3} in the same way as the potential falls of as r^{-3} in three dimensions. In addition to the ϕ^{-3} long range behavior, the potential also contains an oscillating part at smaller distances, which disappear when $\frac{\phi}{2\pi} > 1 + (2\pi)^2 \frac{R}{h}$. The minima in the potential correspond to the dipoles being roughly on top of each other. The period of the oscillations is not 2π, meaning that in the minimum the dipoles are not exactly above each other as it is a compromise in optimizing the angle and the three dimensional distance between dipoles. This oscillating behavior of the potential is not limited to dipolar particles on helix, charged particles confined to move on helix also have an oscillating potential with several minima[33].

The strong nature of the short-range dipole-dipole interaction means that if two dipoles get close, it might cause chemical reactions between them and result in loses from the system. This is not a regime we are interested in and we therefore want to look at a parameter space in which the short range interaction is repulsive. In such a regime we can ignore any chemical reactions and losses following from those. The requirement for the short-range interaction to be repulsive, puts a limit on the shape of the helix. To calculate this limit we note that the denominator in the potential is always positive, so to find the short-range behaivor of the potential it is enough to look at the numerator. The requirement that the short-range interaction is repulsive means that the numerator must also be positive in the limit of $\phi \to 0$

$$0 < (1 - \cos(\phi)) - \frac{h^2}{R^2}\frac{\phi^2}{(2\pi)^2} \tag{2.4}$$

For small values of ϕ the cosine function can be approximated by the first two terms in its power series $\cos(\phi) \approx 1 - \frac{1}{2}\phi^2$. Inserting this into equation 2.4 we get the following requirement on the geometry of the helix

$$\left(1 - \left(1 - \frac{1}{2}\phi^2\right)\right) - \frac{h^2}{R^2}\frac{\phi^2}{(2\pi)^2} > 0 \tag{2.5}$$

This is the case if $\frac{h}{R} < \sqrt{2}\pi$, then the two-dipole potential becomes attractive, and thus we restrict our selves to study cases where $\frac{h}{R} < \sqrt{2}\pi$. With these constrictions on the geometry of the helix a system of two or more dipoles on a helix becomes stable against losses from the chemical reactions that might occur when two dipoles get too close. This stability is one of the reasons why lower dimensional systems of dipoles are of such interest since that is not possible in three dimensions unless som other confinement is introduced.

Chapter 3

Classical Crystals

In this chapter the formation of classical crystals of dipolar particles trapped on a helix is investigated. Such a crystal consist of N dipoles placed on a helix where there position of each dipole is described by the angle ϕ_i. The dipoles are all aligned by an external field. In the first section 3.1 the classical potential energy of N dipoles confined to a helix is calculated. The dipoles tend to form chain like structures long the helix. In section 3.2 the stability of the crystals are investigated through their spectrum of normal modes. Finally in section 3.5 the speed of sound along the chains is calculated. The results shown in this chapter is based on the work in [34]

3.1 Classical Energy

When N dipoles are trapped on helix, the total potential energy of the system can be found as a sum of all the pairwise interactions. The pairwise dipole-dipole interaction was described in the previous chapter, and for two dipoles located at ϕ_i and ϕ_j, it is

$$V(\phi_i,\phi_j)=\frac{d^2}{4\pi\epsilon_0}\frac{2R^2\left[1-\cos\left(\phi_i-\phi_j\right)\right]-2h^2\left(\left(\phi_i-\phi_j\right)/(2\pi)\right)^2}{\left(2R^2\left[1-\cos\left(\phi_i-\phi_j\right)\right]+h^2\left(\left(\phi_i-\phi_j\right)/(2\pi)\right)^2\right)^{5/2}}. \tag{3.1}$$

If the N dipoles on the helix each are located at $\{\phi_k\}$, then the total potential energy is given by the sum

$$E(\{\phi_k\})=\sum_{i<j}^{N}V(\phi_i,\phi_j)\ . \tag{3.2}$$

For each value of N and h/R, the stable crystal configurations are then the different minima of this energy landscape. The corresponding values of $\{\phi_k\}$ are then the equilibrium positions of the dipoles. The two dipole potential in equation 3.1 only depends on the relative distance. The different terms in the fraction all carry unit, we can rewrite it to change this

$$V(\phi_i,\phi_j)=\frac{d^2}{2\pi\epsilon_0}\frac{1}{R^3}\frac{\left[1-\cos\left(\phi_i-\phi_j\right)\right]-\left(\frac{h}{R}\right)^2\left(\left(\phi_i-\phi_j\right)/(2\pi)\right)^2}{\left(2\left[1-\cos\left(\phi_i-\phi_j\right)\right]+\left(\frac{h}{R}\right)^2\left(\left(\phi_i-\phi_j\right)/(2\pi)\right)^2\right)^{5/2}}. \tag{3.3}$$

From this we also get the unit of energy that we get when we calculate the total potential energy in equation 3.2, namely $\frac{d^2}{2\pi\epsilon_0 R^3}$. We reiterate that the short range interaction between two dipoles on a helix becomes attractive if $\frac{h}{R}>\sqrt{2}\pi$ and that this is a regime that we are not interested in. So we will restrict our selves to the cases where $\frac{h}{R}<\sqrt{2}\pi$.

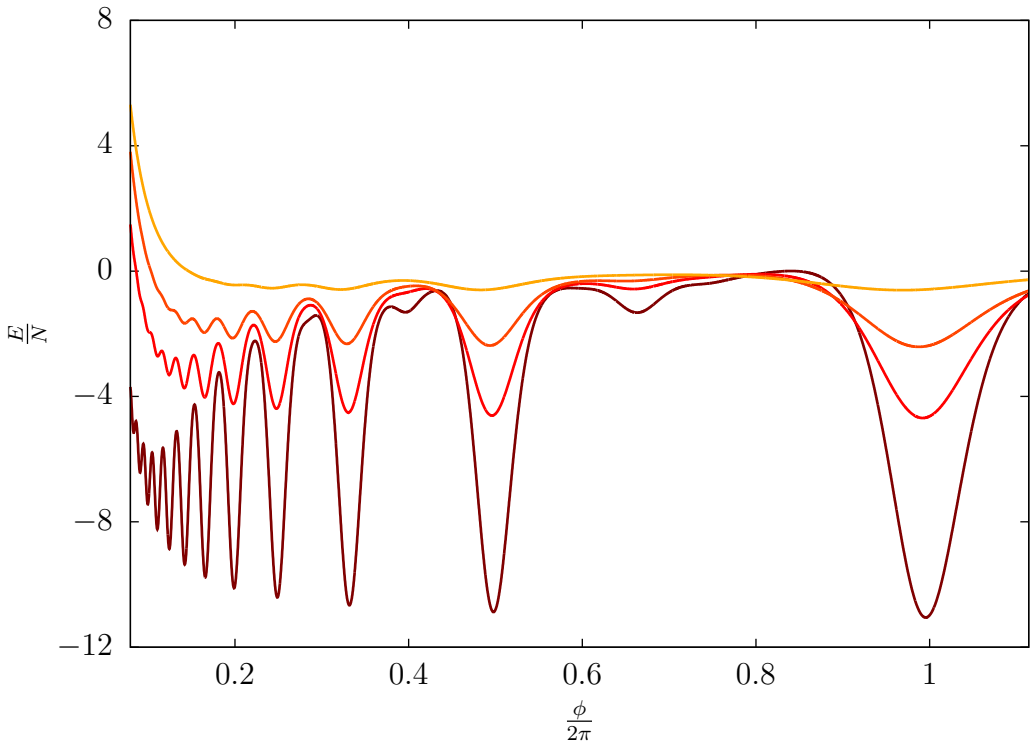

Figure 3.1: The reduced energy per particle, E/N, in units of $d^2/(2\pi\epsilon_0 R^3)$ as function of the fixed angular distance, ϕ, between the particles. The different curves correspond to $h/R = 1.6, 1.0, 0.8$ and 0.6 with smaller well depths for decreasing h/R. The total particle number is $N = 100$.

.

Equilibrium configurations

A full coordinate variation of all the positions requires a minimization of an N-dimensional function, which depending on N can be a daunting task. To simplify the problem there are various constraints that could be imposed on the system. The first such constraint is to assume that all the dipoles are equally spaced along the helix, that is the angular distance between two neighboring dipoles $\phi = |\phi_i - \phi_j|$ is constant. For a fixed number of dipoles N this would correspond to varying the length of the helix. The resulting energy per particle is shown as function of the dipole separation ϕ in figure 3.1. The most striking feature of figure 3.1 is the oscillatory behavior. All the minima at shorter and shorter angular separation between the dipoles correspond to an increasing number of dipoles per winding. The figure cuts off at a separation just larger than a single winding, but the oscillations continue for larger separation with a new minima at each multipla of 2π but with a cubic decrease of the depth. These configurations correspond to the dipoles being more than a single winding apart. The depth of the different minima are roughly equal for the four largest dipole separations in figure 3.1, but for smaller separation, the depth decreases, before becoming strictly repulsive. To interpret these features, it is useful to recall that the dipole-dipole interaction is attractive when the dipoles are arranged head-to-tail, and repulsive when the dipoles are arranged side-by-side. The results in figure 3.1 suggest that the energy is dominated by the attraction between dipoles in different windings.

If one takes a closer look at the minimum at $\phi \approx 2\pi$, one can see that the h/R

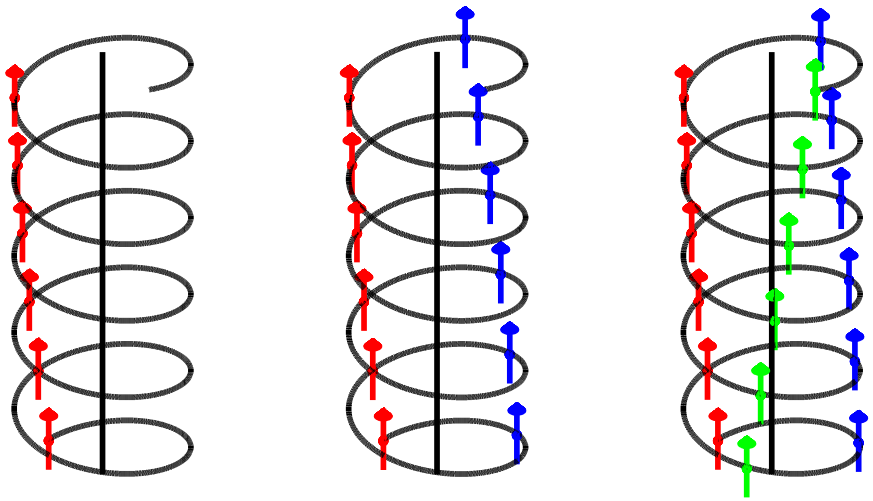

Figure 3.2: Schematic drawings of chain configurations on a helix. Left is one chain, middle two chains asymmetrically located along the helix, right is three chains. To guide the eye the dipoles in each chain have the same colors.

dependence of the location is very small but it is non-zero. The location of the minimum is not exactly 2π, in fact it is slightly less than 2π. This means that the dipoles are not exactly one winding apart, and thus the position of the dipoles along the chain on the helix slowly rotates around the axis. In the case of $\frac{h}{R}$ it is after about 75 layers a full revolution of 2π is completed. The second minimum corresponds to two dipoles per revolution, again it is not exactly one revolution and the two chains of dipoles rotates around the helix on opposite sides. In figure 3.2 one can see a drawing of the chain configurations on a helix. Each of the three configurations shown in figure 3.2 corresponds to a minimum in figure 3.1. In figure 3.2 one can clearly see how the chains rotate around the helix. The drawing is not large enough to see a full rotation around a helix but one can imagine how it would look. The dipoles belonging to the same chain have been colored in the same color this is only to guide the eye. The color does not represent any physical property. The energy per particle on the helix varies with both the dipole separation, and the ratio of the height and radius of the helix h/R. In three dimensions the energy between two dipoles scales as r^{-3}. For dipoles separated by one winding the three dimensional distance scales as h, and thus from dipole-dipole potential we get that the energy must scale as h^{-3}. This means that if it is the interactions along a single chain that dominate the total energy, then the total energy is expected to scale in the same way. The expected scaling is shown in figure 3.3. In the figure the product $\frac{E}{N}\left(\frac{h}{R}\right)^3$ is shown as a function of $\frac{h}{R}$. That product is then expected to be

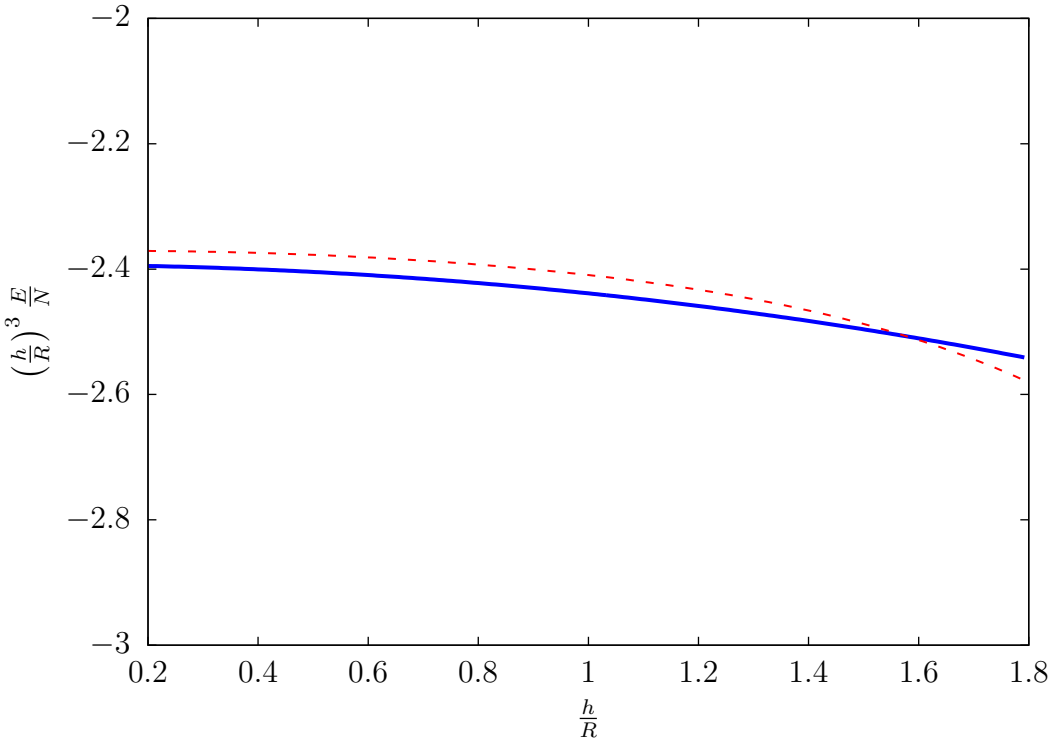

Figure 3.3: Reduced energy per dipole multiplied by $(h/R)^3$ as a function of the ratio $\frac{h}{R}$ for one (full blue) and three (dashed red) dipoles per revolution.

constant under the assumption that the in-chain interactions are dominating. On the scale shown in figure 3.3, with $0.2 < \frac{h}{R} < 1.8$ it only varies by about 10%. This variation is mostly because the two-dipole potential changes shape as a function of $\frac{h}{R}$ and thus the equilibrium distance between two dipoles does not exactly scale as h^{-3}. If $\frac{h}{R}$ becomes too larger then the attraction between dipoles in different chains and different windings increases and this explains the difference in the scaling for one and three chains on the helix. We will later show that the two-chain configuration becomes unstable. Its scaling is not shown in figure 3.3. This picture of chains of dipoles along the helix has some interesting consequences on the normal modes of these equilibrium configurations.

3.2 Normal modes and stability

A way to further study systems of dipoles on a helix is to calculate the normal modes and frequencies of the vibrations of the dipoles, around their equilibrium configurations.

$$E - E_0 \approx \frac{1}{2}\sum_{i,j} K_{i,j}(\phi_i - \phi_i^{(0)})(\phi_j - \phi_j^{(0)}) \,, \tag{3.4}$$

$$K_{i,j} = \frac{\partial^2 E}{\partial\phi_i \partial\phi_j} \,, \tag{3.5}$$

Here E_0 is the equilibrium energy. The first order derivatives are omitted since in equilibrium they will not contribute. The second order derivatives in the matrix K are all calculated at the equilibrium. By diagonalizing the matrix K one performs a change

of variables into a set of normal modes that describes the vibrations of the dipoles. The eigenvalues found are $\frac{1}{2}m\omega_n^2$, where ω_n^2 are the frequencies of the corresponding normal modes. The frequencies ω_n^2 are positive if the equilibrium configuration $\{\phi_j^{(0)}\}$ is stable. Conversely if the frequencies are negative then the equilibrium configuration is not stable.

Simple models

The restoring force on dipoles towards the equilibrium is found from the energy in equation 3.4. As long as the vibrations are not too far away from equilibrium the calculations are sufficiently accurate to the second order. For large N the dependence on the end points should vanish and the effect seen in section 3.4 in the difference between 12 and 13 dipoles will be negligible. With the dipoles equally spaced along the helix there is a translational symmetry. First, because there is no external potential along the helix a translation of all the dipoles does not change the energy. Secondly all the two body properties only depend on the relative distance between the dipoles not the absolute position of the dipoles on the helix. This means that entries in the matrix $K_{i,j}$ has to be the same as $K_{i+k,j+k}$ for any k. The double sum in equation 3.4 can now be performed over a constant sum, k and a constant difference, l. It is however only the relative distance that matters for the energy. Instead of using the absolute positions of the dipoles along the helix as the coordinates it is useful to introduce the distance each dipole is away from its equilibrium position $\tilde{\phi}_i = \phi_i - \phi_i^{(0)}$. This leads to the following expansion of the energy

$$E - E_0 = \sum_{l>0} \frac{1}{2} K_{k+l,k-l} \left(\tilde{\phi}_{k+l} - \tilde{\phi}_k\right) \left(\tilde{\phi}_{k-l} - \tilde{\phi}_k\right) \ . \tag{3.6}$$

The force on dipole k is then minus the gradient of the potential energy given by equation 3.6. According to Newtons second law this equal to the mass times the acceleration, and the equation of motion becomes

$$m\frac{\partial^2 \tilde{\phi}_k}{\partial t^2} = \frac{1}{2} \sum_l K_l (\tilde{\phi}_{k+l} + \tilde{\phi}_{k-l} - 2\tilde{\phi}_k) \ , \tag{3.7}$$

Here the notation $K_l = K_{k+l,k-l}$ is introduced. Because we are searching for vibrational motion we use the ansatz the each dipole undergo periodic motion around the equilibrium, that is $\tilde{\phi}_j = A_j \cos(\omega_j t + a_j)$. With equal amplitudes $A_j = A_0$ and an average phase $(a_{k-l} + a_{k+l})/2 = a_k$ for all l, which means the phase has to be linear $a_j = b_0 + jb_1$, the time dependencies cancels out and we get an equation for the frequencies

$$\begin{aligned} m\omega^2 &= \sum_l K_{l>0}(1 - \cos(lb_1)) \\ &= 2\sum_l K_{l>0} \sin^2(lb_1/2) \ . \end{aligned} \tag{3.8}$$

The frequencies along with the phases characterize the N independent solutions. By adding periodic boundary conditions, which works for sufficiently large N, one gets a discrete set of phases and $b_1 = 2\pi n/N$ with n any integer smaller than N. We get N solutions with frequency ω_n. The size of K_l decreases strongly with l seeing as the dipole-dipole interaction falls of cubicly. Which order is largest depends on the number

of chains seeing as a dipole interacts the strongest with those directly above and below it. Thus for one chain of dipoles on the helix K_1 is the largest. Expanding the expression for the frequency we find that

$$\omega_n \approx \frac{2\pi n}{N}\sqrt{\sum_{l>0} l^2 K_l/m}\ . \tag{3.9}$$

The speed of sound, c, is then obtained as the ratio between ω_n and the wave number k_n. The latter is found by equating the total length of the helix with the wave length. Thus, $RN(\Delta\phi)_0 = 2\pi n/k_n$ where $(\Delta\phi)_0$ is the angular distance between the equidistantly placed dipoles. We then finally get

$$c = \frac{\omega_n}{k_n} \approx R(\Delta\phi)_0\sqrt{\sum_{l>0} l^2 K_l/m}\ , \tag{3.10}$$

3.3 Stability

For a given configuration of dipoles $\{\phi_j^{(0)}\}$, the elements of the K-matrix is calculated analytically from the two-dipole potential in equation 3.1. The matrix is then diagonalized, and the full spectrum is calculated. The matrix is diagonalized numerically and the eigenfrequencies and the eigenvectors then contain all N angular coordinates. This is in contrast to the energy calculations done in section 3.1 where the only coordinate is the nearest-neighbor separation ϕ. By increasing the size of the configuration space we open up to instabilities coming from modes that do not keep the nearest-neighbor separation the same between all dipoles. The presence of an imaginary frequency(negative ω_n^2 implies imaginary ω_n) does not tells what the true equilibrium configuration is, but the corresponding normal mode will give some hint to what it might look like.

It turns out that not all the equilibrium configurations corresponding to the minima in figure 3.1 are stable. The stability of these configurations depends on both the geometry of the helix, that is $\frac{h}{R}$ and on the total number of dipoles N. One dipole per revolution is a stable configuration as long as the short-range interaction is repulsive, i.e that $\frac{h}{R} < \sqrt{2}\pi$. For two-, three- and four dipoles per revolution it is not as simple and it is worth it to investigate stability of these configurations. Using the minima of figure 3.1 as a starting point, we consider equidistant configurations of two, three and four dipoles per revolution. The nearest-neighbor distance between the dipoles are $\phi \approx \pi$, $\phi \approx 2\pi/3$ and $\phi \approx \pi/2$, respectively. Then the total number of dipoles is increased, and we check when these configurations become unstable, or if they stay stable. Then one can define the critical number of dipoles N_{crit} of a certain configuration, as the number of dipoles at which the configuration becomes unstable. In figure 3.4 the critical number of dipoles is shown as a function of $\frac{h}{R}$ for a system of two, three or four dipoles per revolution. If there is no point for a particular value of $\frac{h}{R}$ that means that this particular system is stable up to at least the maximum size that we considered namely $N = 1600$. The equidistant configuration of two dipoles per revolution is stable when $\frac{h}{R} < 0.65$. For larger values of $\frac{h}{R}$ smaller than 0.65 the configuration becomes unstable and N_{crit} becomes smaller as $\frac{h}{R}$ increases. For three dipoles per winding the behavior is different. N_{crit} decreases as $\frac{h}{R}$ increases from 0.5 to 0.9 at which point the equidistant configuration suddenly becomes stable(at least up to $N = 1600$). Four Dipoles per winding is similar to three dipoles per winding except stability already occurs at $\frac{h}{R} > 0.6$.

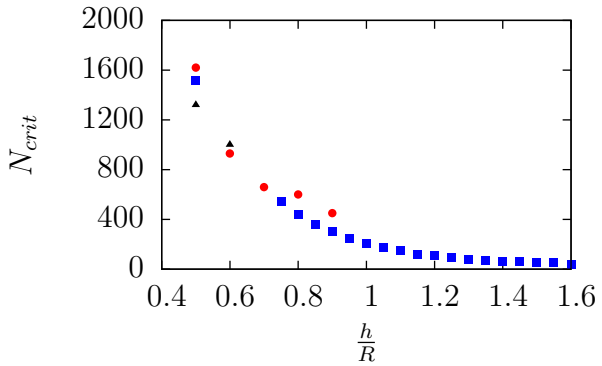

Figure 3.4: The critical number of dipoles N_{crit} as a function of $\frac{h}{R}$. For $N > N_{crit}$ the equidistant configuration becomes unstable. The blue square is for two dipoles per winding, the red circle is with three dipoles per winding and the black triangle is for 4 dipoles per winding

Chain structure

It turns out that the chain structure of the dipoles is key to understand the stability of the dipoles on a helix. Looking back at the three minima in figure 3.1 corresponding to one, two or three dipoles per winding, these three configuration are shown in figure 3.2. In the figure we see the different chains rotating around the helix. We first focus on the stability of the configuration of the two dipoles per winding configuration. Looking at two neighboring dipoles belonging to different chains, their interaction changes for repulsive to attractive as $\frac{h}{R}$ increases. This leads the equidistant configuration to become energetically unfavorable. The stability of the chain depends on the total number of dipoles on the helix. To explain this we look at what happens when one adds another pair of dipoles to the helix. The two dipoles are added to the different chains and thus repel each other, but they are attracted to most of the dipoles in the other chain below it. This happens since angle between them approaches the head-to-tail configuration as the number of windings between them increase. For a larger number of dipoles, the number of these attractions increase. this is what causes the two chain configuration to become unstable.

We test this explanation of the instability by calculating the energy per dipole as a function of the distance between the two chains shown in figure 3.2. The energy per particle is shown in figure 3.5, a separation of the two chains by approximately $\phi \approx \pi$ corresponds to the equidistant minimum configuration in figure 3.1. This is calculated for the unstable case of $N = 500$ dipoles in two chains for the case of $\frac{h}{R} = 1$. We see that equidistant configuration corresponds to a local maximum, and that there are two identical minima at $\phi = 1.8$ and $\phi = 4.3$. There are two minima because there is no difference between whether a dipole is close to its neighbor above it or the one below. This strongly suggest that the true equilibrium configuration is one where the chain structure remains but the two chains are moved close to each other. Another argument in favor of this two chain interpretation is that the first unstable normal mode, is the one where the two chains vibrate in opposite directions. We have calculated the spectrum of normal modes for this new configuration, and it show stability even for large N.

This result from two chains on a helix we use as a starting point for another case that showed instability in figure 3.4. Namely the case of three chains and $\frac{h}{R} = 0.6$, where the equally spaced configuration becomes unstable for $N > N_{crit} \approx 900$. We start out

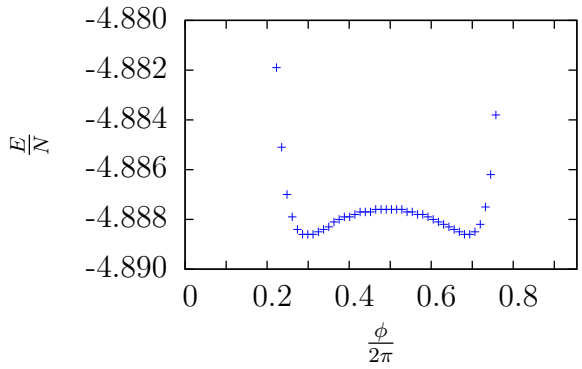

Figure 3.5: The reduced energy per dipole, E/N, as function of the angular distance between two chains of dipoles for $N = 500$ and $h = R$.

by placing two chains with an angular separation of $\frac{4}{3}\pi$, and place the third chain in between them in correspondence with the minimum in figure 3.1. The position of the third chain is then varied and we calculated the energy per dipole for three different total sizes as a function of the position of the third chain in figure 3.6. For a total number of dipoles $N = 500 < N_{crit}$ we see a single minimum at $\frac{4}{3}\pi$ directly between the other two chains. This is in accordance with the equidistant configuration being stable for this size. For $N = 700$ it is not easy to spot the minimum by eye, but increasing it to $N = 1000$, there is clearly two separate minima on opposite sides of the now unstable equidistant configuration. This is similar to the previously discussed case of two chains. This chain structure interpretation is again supported by the observation that the normal mode with the unstable imaginary frequency is the one where the three chains vibrate against each other. The discussion in this section shows that even when the equidistant configuration becomes unstable, we can recover the chain structure by moving the chains closer since by doing this the system again becomes stable.

3.4 Small systems

The previous discussion shows that the long-range part of the dipole-dipole interaction is responsible for many of the features of the structures of dipoles on a helix. The attraction between dipoles that are many windings apart leads to the large N instability of the equidistant configurations. By looking at systems with a smaller number of dipoles the systems become stable and it becomes easier to visualize the different normal modes.

The first system to study is $N = 12$, this is chosen because it is divisible with both 2,3 and 4 dipoles per winding. With an equal number of dipoles in each chain we expect a clean spectrum of normal modes. We show all squared frequencies in the upper panel of figure 3.7, for both 2,3 and 4 dipoles per winding. It is very striking that each of the systems show either a two-, three- or fourfold degeneracy. This degeneracy is because the chains are of equal size. The degeneracies becomes less pronounced as the frequencies increase. These features are again because of the chain structure. For two chains on the helix, the two degenerate modes correspond to the same in chain vibrations, but the relative vibrations between the chains change, either they vibrate in phase, or they vibrate against each other. The amplitudes for the lowest degenerate set of normalmodes are shown in the bottom panels of figure 3.7.

For two chains on the helix the bottom left panel in figure 3.7 shows eigenmode

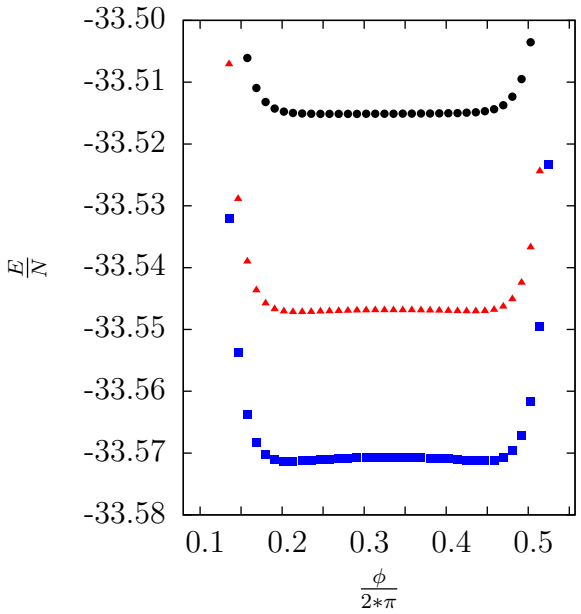

Figure 3.6: Reduced energy per dipole, $\frac{E}{N}$, as a function of the position of a third chain of dipoles between two other chains, the first two chains are separated by $\phi = \frac{2}{3}2\pi$ radians, and the position of the third is measured from the first. This is done from top to bottom for $N = 500$ (black circle) $N = 700$ (red triangle) and $N = 1000$ (blue square) dipoles and $\frac{h}{R} = 0.6$.

number 3. It shows that neighboring dipoles move out of phase, that is the two chains vibrate against each other, but it also shows a node in the vibrations along the chain. This is the two dipoles at opposite ends of a chain that vibrate against each other. The middle panel show the fourth eigenmode where the two chains vibrate in phase, but like the third mode there is a node in the in-chain vibration such that the ends of the chain vibrate against each other. In general this implies that the vibration can be written as a product of two independent types of vibrations, the in-chain vibration, and the relative vibrations between the chains. For three chains the bottom panels show mode number 4, 5 and 6. The bottom left panel shows two of the chains vibrating against the third chain. One can see that the two chains vibrating in phase have half the amplitude of the other chain. The bottom middle panel show all the chains vibrating in phase. In the bottom right panel we are back to two chains vibrating against the third. For four dipoles per winding for which the normal modes are not shown in figure 3.7, the normal modes show a similar structure with all the chains moving in phase, or one or two chains moving against the other chains. The degeneracies are because of the relatively weak interaction between the different chains, but we see the higher the frequency the less pronounced the degeneracy because of the increased importance of the interaction between the chains.

The simple structures in the spectrum arise because of how 12 dipoles were chosen such that there would always be an integer number of dipoles per chain. If this was not the case, then the degeneracies would be lifted, and the spectrum changes. The symmetry between the different chains are lifted by adding a thirteenth dipole. The dipoles still form chains, the dipole is just added to the end of one of the chains which then becomes longer than the other chains. In figure 3.8 the eigenfrequencies for the $N = 13$ case is shown for 2,3 and 4 chains respectively, and in each case with one of the

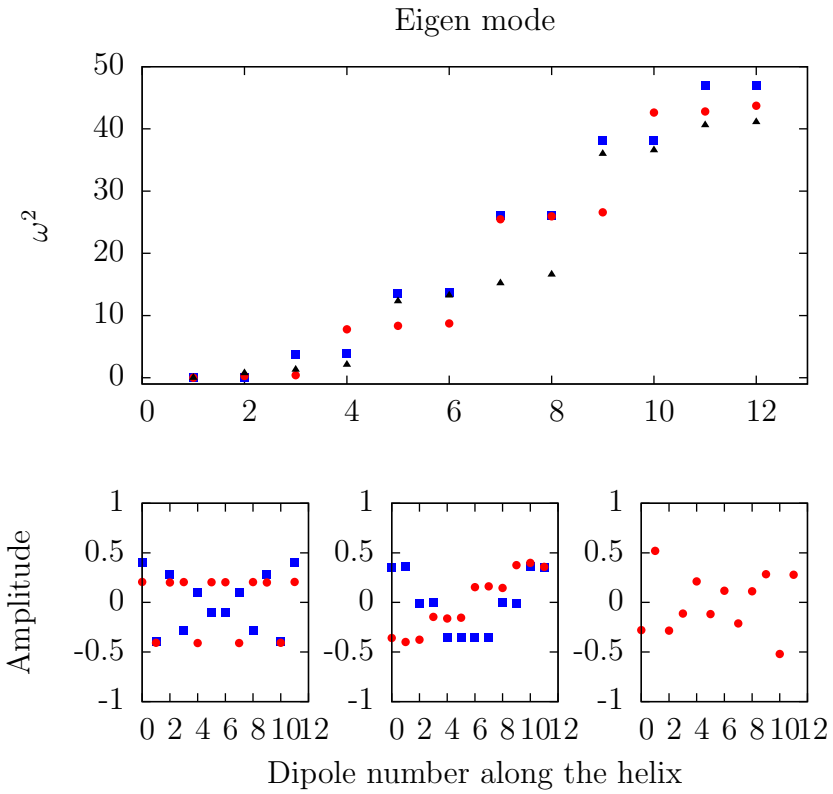

Figure 3.7: (top) The spectrum of squared frequencies for 12 dipoles, with two (blue square), three (red circle) and four (black triangle) dipoles per revolution. (bottom) The amplitudes of the normal modes for the lowest nearly degenerate eigenvalues. Left is eigenmode number 3 (blue square) and 4 (red circle), respectively for two and three dipoles per windings. Middle is eigenmode number 4 (blue square) and 5 (red circle), respectively for two and three dipoles per windings. Right is eigenmode number 6 (red circle) for three dipoles per windings.

chains having an extra dipole. Compared to the $N = 12$ case the degeneracies are now gone. The two bottom panels show the third and fourth eigenmode for two chains. Both modes show one of the chains essentially sitting still while the other chain undergoes a vibration with a single node. The difference between the two modes is which of the two chains is undergoing the motion. This boundary effect of adding an extra dipole that then lifts the degeneracy between the normal modes would decrease is the total number of dipoles is increased.

3.5 Speed of sound

The speed of sound in a crystal is a fundamental property, that is important for several physical properties of the crystal. The sound wave is a propagation of vibrations along the crystal, and the spectrum of normal modes contain all the necessary information needed to calculate it. The total length of the crystal discussed in this chapter is $NR\,(\Delta\phi)_0$, where $(\Delta\phi)_0 = \phi_{i+1} - \phi_i$ is the nearest neighbor separation between the dipoles. As discussed in the introductory section on normal modes (section 3.2. The speed of sound is given by the ratio $c = \frac{\omega_n}{k_n}$ in the limit of small k_n. To reach the limit of small k_n we have to move towards large systems since $k_n = \frac{2\pi n}{NR(\Delta\phi)_0}$.

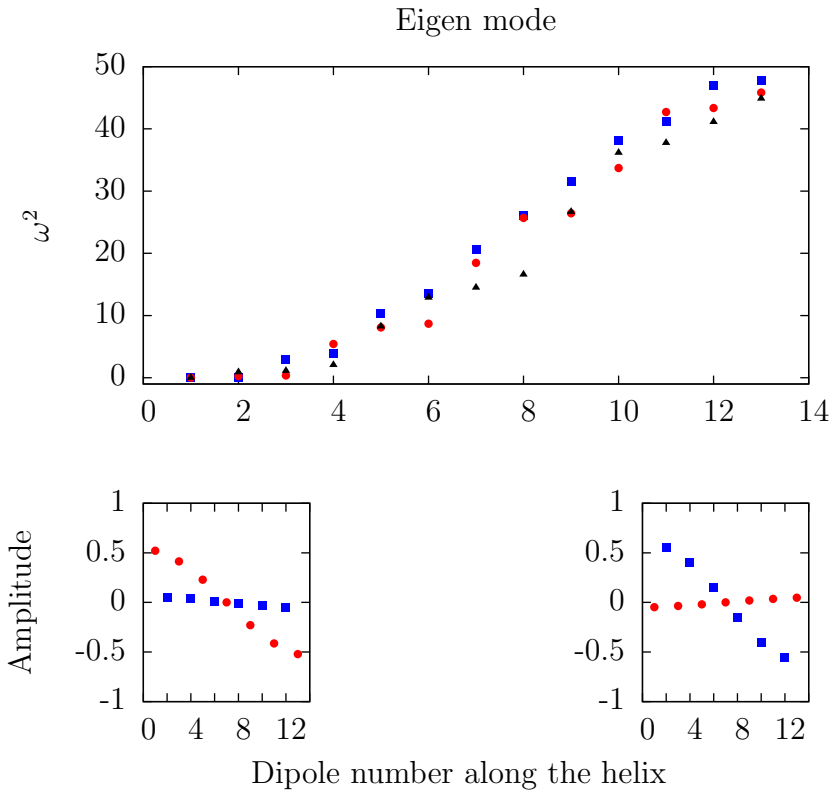

Figure 3.8: (top) The spectrum of squared frequencies for 13 dipoles, with two (blue square), three (red circle) and four (black triangle) dipoles per revolution. (bottom) The amplitudes of the normal modes for the lowest nearly degenerate eigenvalues of two dipoles per winding. Left is eigenmode number 3 where the long chain (red circle) is moving while the short chain (blue square) remains at rest. Right is eigenmode number 4 where the chains exchange motion.

Numerical results

For each choice of 1, 2, 3 and 4 dipoles per winding all N eigenfrequencies ω_n are calculated. This is done for the stable equidistant configurations. In figure 3.9 the ordered frequencies are shown for $N = 20, 50, 100$ and $h = R$. Note that for these choices of N and $\frac{h}{R}$ all systems are stable as shown in figure 3.4. The x-axis in figure 3.9 is scaled with the total number of dipoles N. The details of the specific eigenvalues are not visible in this figure, but the striking feature of this plot is that all the frequencies follow the same curve after they have been scaled. All the configurations have the squared frequency vary from zero up to about 50. Looking to the models in section 3.2 we see from equation 3.8, where b_1 varies from 0 to 2π, that the maximum limiting the largest frequencies is the sum of the curvatures. This sum is independent of N as the interactions between the dipoles fall off fast with increased distance. Another interpretation of this is that the highest frequency modes are the ones where two neighbors within a chain vibrate out of phase, and this type of vibration is independent of the number of chains and the length of the chain.

We now turn back to the lowest frequencies, as they are the ones that determine the speed of sound c. They are expected to vanish as n/N for increasing N. By calculating the entire spectrum for several values of N and then multiplying the lowest frequencies by N/n, one would expect a constant. In figure 3.10 the three lowest frequencies are

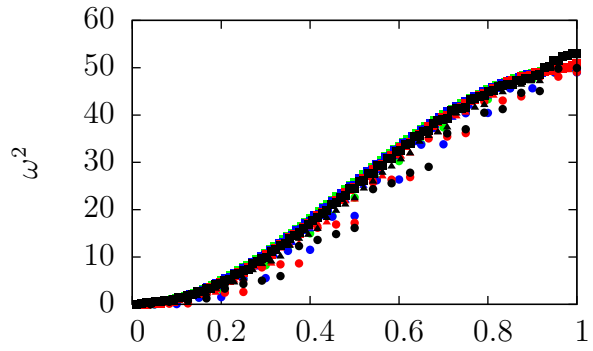

Figure 3.9: The squared eigenfrequencies with $h/R = 1$ for $N = 20$ (circle), 50 (triangle), and 100 (square) as functions of their number in the ordered sets of eigenvalues divided by the total number of dipoles. The dipoles per revolution are 1 (green), 2 (blue), 3 (red), and 4 (black). The unit is $d^2/(4\pi\epsilon_0 m R^3)$.

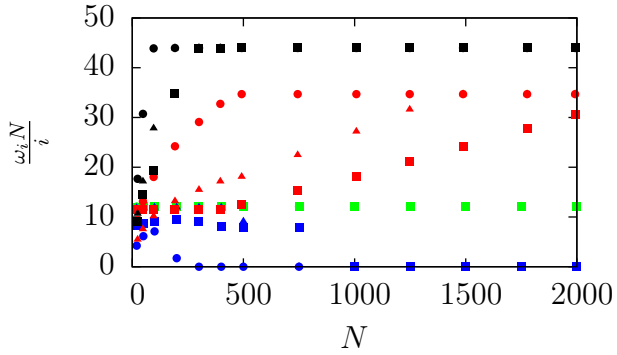

Figure 3.10: The lowest three eigenfrequencies multiplied by N and divided by respectively 1 (circle), 2 (triangle), and 3 (square) exhibited as functions of N. We choose $h = R$ and the number of dipoles per revolution to be 1 (green), 2 (blue), 3 (red), and 4 (black). The unit is $(d^2/(4\pi\epsilon_0 m R^3))^{1/2}$.

shown multiplied by N/n as function of N. For 1, 3 and 4 dipoles per revolution they all enter the expected regime of scaling with n/N, but for two dipoles per revolution(the blue points) we see a very noticeable deviation. For two dipoles per revolution we see an increase for small values of N and then a drop off. This is because the equidistant configuration becomes unstable as has been previously discussed.

Finally we calculate the speed of sound c. This is done by taking the limits in figure 3.10, and multiplying them by $R\left(\Delta\phi\right)_0/(2\pi n)$. The results of this are shown in figure 3.11 for $n = 1$ as a function of h/R. For one dipole per revolution, the speed of sound follows what appears to be a smooth curve. The speed of sound decreases roughly as $(R/h)^3$ which is similar to the scaling of the energy shown in figure 3.3. For more than one chain, a similar scaling is seen. However, due to instabilities at large N there are fewer points than for only one chain. It is very striking that all the points for stable configurations follow the same curve as for only one chain. Referring back to the model, we have that $\left(\Delta\phi\right)_0$ decreases when the number of dipoles per revolution is increased, but this is balanced by the factor l^2 inside the square root in equation 3.10. The K_l that dominates the sum are the ones that refer to dipoles in the same chain. So if one

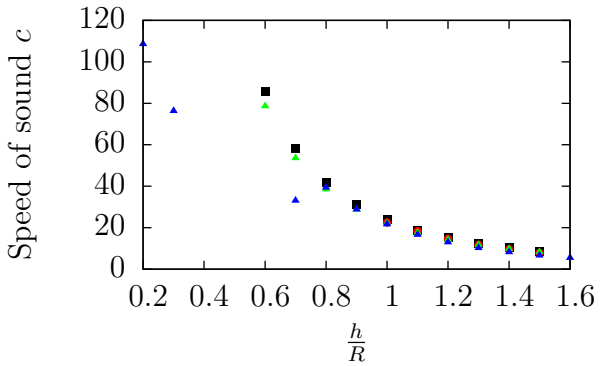

Figure 3.11: The Speed of sound c obtained for $n = 1$ as a function of the ratio $\frac{h}{R}$ for one dipole per revolution (black square), three dipoles per revolution (red circle), four dipoles per revolution (blue nabla) and a nearest-neighbor calculation for 1 dipole (green triangle)

doubles the number of chains on the helix, $(\Delta\phi)_0$ is halved. But the l that corresponds to the dominating K_l is doubled, and the effects cancel out.

3.6 Summary

We calculated the classical potential energy of N dipoles distributed uniformly on a helix. This lead to several configurations of roughly the same energy per dipole. These different configurations all corresponded to a different number of chains along the helix. Within each chain the dipoles were arranged in a head-to-tail manner. We investigated the stability of these equidistant chain structures as a function of the total number of dipoles N and the pith-to-radius ratio $\frac{h}{R}$. We showed to for certain values of these parameters the equidistant configurations became unstable and the chains tended to cluster together. The stability was also investigated through a calculation of the vibrational normal modes, these calculations also revealed that when the equidistant configurations became unstable it was the mode that corresponds to the chains moving against each other which had a imaginary frequency. We also studied smaller systems of $N = 12$ and $N = 13$ dipoles. The number 12 was chosen as it allowed for symmetric configurations of 2, 3 and 4 chains of dipoles. This symmetry lead to a degenerate set of normal modes. The degeneracy was then lifted by adding another dipole to the system.

Chapter 4

Numerical Methods

In this chapter we introduce the two different methods we use to solve the Schrödinger equation.

4.1 Grid based methods

The first class of methods we will discuss are the grid based methods. We start by looking at the one dimensional Schrödinger equation for a wire of finite length. To discretize the problem of solving the one dimensional Schrödinger equation, we create a set of basis functions $\phi_i(x)$ that are located on a grid of N different points $x_i....x_N$. Here each of the points are separated by the distance Δx. The basis functions are defined as follows:

$$\phi_i(x) = \begin{cases} \frac{1}{\sqrt{\Delta x}} & \text{for } x \in \left[x_i - \frac{\Delta x}{2}, x_i + \frac{\Delta x}{2}\right] \\ 0 & \text{for } x \notin \left[x_i - \frac{\Delta x}{2}, x_i + \frac{\Delta x}{2}\right]. \end{cases} \tag{4.1}$$

We the approximate integrals of functions by sums over all the grid points, that is

$$\int_{x_1}^{x_N} F(x)dx = \sum_i F(x_i)\Delta x. \tag{4.2}$$

This turns the inner product between two basis states into

$$\langle \phi_i | \phi_j \rangle = \delta_{ij} \tag{4.3}$$

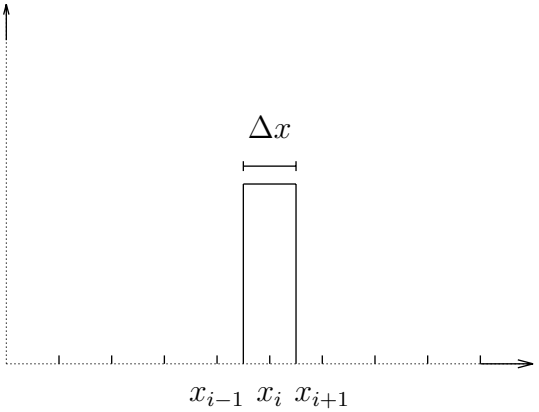

Figure 4.1: One of the functions in the basis centered at x_i.

The set of functions defined on the grid thus forms an orthonormal set of basis functions defined on the line. The matrix elements of the potential in the Schrödinger equation $H = T + V$ is given by

$$\langle \phi_i | V | \phi_j \rangle = V(x_i)\delta_{ij} \tag{4.4}$$

This means that the potential can be represented by a diagonal matrix where the diagonal is the value of the potential at each grid point.

$$\langle \phi_i | V | \phi_j \rangle = \begin{bmatrix} V(x_1) & 0 & 0 & ... & 0 & 0 \\ 0 & V(x_2) & 0 & ... & 0 & 0 \\ . & . & . & ... & . & . \\ . & . & . & ... & . & . \\ 0 & 0 & 0 & ... & V(x_{N-1}) & 0 \\ 0 & 0 & 0 & ... & 0 & V(x_N) \end{bmatrix}. \tag{4.5}$$

For the kinetic energy term it is a bit more involved, as it includes a second order derivative. This second order derivative can be approximated by

$$\frac{\partial^2 \phi_j(x_k)}{\partial x^2} = \frac{\phi_j(x_{k+1}) - 2\phi_j(r_k) + \phi_j(x_{k+1})}{\Delta x^2} = \frac{\delta_{j,k+1} - 2\delta_{j,k} + \delta_{j,k-1}}{\Delta x^{5/2}} + O(\Delta x^4). \tag{4.6}$$

This turns the kinetic energy operator into a tri-diagonal matrix:

$$\langle \phi_i | T | \phi_j \rangle \approx \frac{1}{2\Delta x^2} \begin{bmatrix} -2 & 1 & 0 & ... & & 0 & 0 \\ 1 & -2 & 1 & ... & & 0 & 0 \\ . & . & . & ... & & . & . \\ . & . & . & ... & & . & . \\ 0 & 0 & 0 & ... & 1 & -2 & 1 \\ 0 & 0 & 0 & ... & 0 & 1 & -2 \end{bmatrix} \tag{4.7}$$

The derivatives at the edges only depend on the point on the inside of the line. This corresponds to the function being zero on the grid points x_0 and x_{N+1}. These boundary conditions work well when one is looking for bound states where the wavefunction is assumed to be localized. The total Hamiltonian $H = T + V$ is thus a tridiagonal matrix which can then be diagonalized by standard matrix libraries.

Convergence

The question is how the eigenvalues of the lowest lying states depend on the choice of N and Δx. We first investigate the convergence as a function of the number of grid points N. In figure 4.2 the two lowest eigenvalues are plotted as a function of N for a fixed value of $\Delta x = 0.02$. We see a sharp convergence for both of the two states because the dependence on N is on whether $N \cdot \Delta x$ is large enough so that the assumption that the wavefunctions are zero at the edge of the box is accurate. That is also why the first excited state requires a larger N than the lowest state. In figure 4.3 the value of the two lowest eigenvalues is shown as a function of the grid spacing Δx. We see that for very small Δx the calculations break down. This is the same reason as in figure 4.2 namely that the product $N \cdot \Delta x$ is so small that the boundary conditions are poorly reproduced. But for larger Δx we see that energies become worse. For the lowest state we see that we need $\Delta x < 0.1$ to get a nice convergence, but one has to be careful such that the product $N \cdot \Delta x$ is sufficiently large such that the assumption that the wavefunction goes

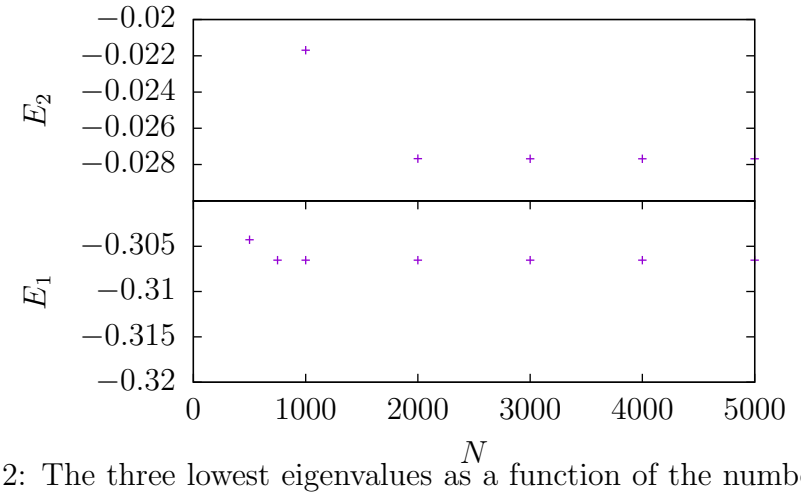

Figure 4.2: The three lowest eigenvalues as a function of the number of grid points N. This is calculated with a fixed grid size $\Delta x = 0.02$.

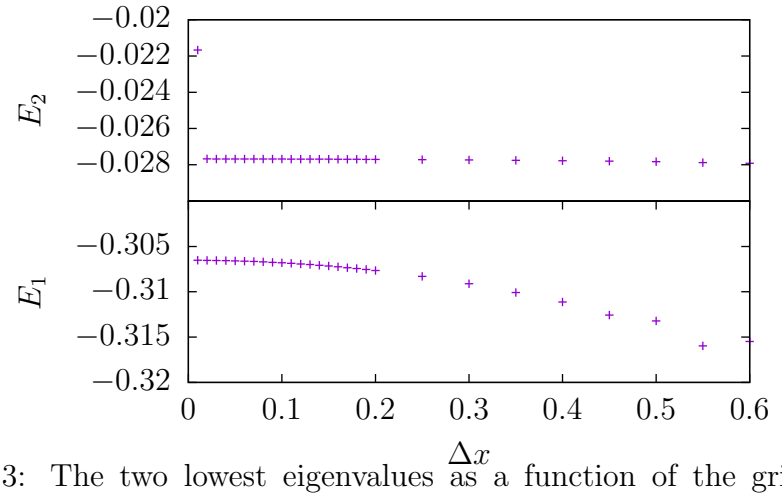

Figure 4.3: The two lowest eigenvalues as a function of the grid size Δx. This is calculated for a fixed number of grid points $N = 2000$.

to zero at the boundary is accurate. One can see that the energy of the higher lying state is much less dependent on the size of Δx. The eigenfunction of E_1 is expected to be more localized than that of E_2, and that is why it is for E_2 we see the breakdown for very small Δx, since with N constant then the size of the box $N \cdot \Delta x$ becomes too small and the boundary conditions becomes inaccurate.

Three particle Schrödinger equation

Introducing a third particle on the helix adds another relative coordinate to Schrödinger's equation. This turns it from a one dimensional problem into a two dimensional problem to solve in the two relative coordinates x and y. The two dimensional problem can again be solved by discretizing it and solving it on a grid. The basis function are now of the form

$$\phi_i(x,y) = \begin{cases} \frac{1}{\sqrt{\Delta x \Delta y}} & \text{for } x \in \left[x_i - \frac{\Delta x}{2}, x_i + \frac{\Delta x}{2}\right] \text{ and } y \in \left[y_i - \frac{\Delta y}{2}, y_i + \frac{\Delta y}{2}\right] \\ 0 & \text{Otherwise.} \end{cases} \tag{4.8}$$

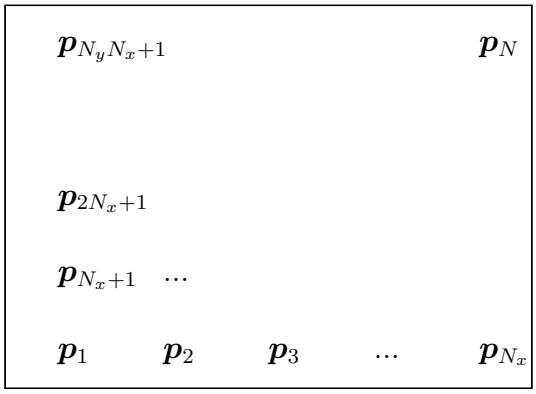

Figure 4.4: An illustration of how the numbering of grid point work for a two dimensional basis.

The numbering of the grid points goes from $1...N$ as shown in figure 4.4. In the figure we see how the numbering starts in one corner and goes row by row to the end from $\boldsymbol{p}_1 = (x_1, y_1)$ to $\boldsymbol{p}_N = (x_N, y_N)$: Integrals are calculated in the same way as in the one dimensional case, where we approximated them by a finite sum over all the grid points.

$$\int_{x_1}^{x_{N_x}} \int_{y_1}^{y_{N_xN_y+1}} F(x)dxdy = \sum_i F(\boldsymbol{p}_i)\Delta x\Delta y \tag{4.9}$$

Using this definition of the integrals one can show that it forms an orthonormal basis. The matrix elements of the potential term is calculated in the same way. The matrix element of the potential term is still diagonal

$$\langle \phi_i | V | \phi_j \rangle = V(x_i, y_i)\delta_{ij} \tag{4.10}$$

The kinetic energy term changes as there are now both T_x and T_y. T_x behaves just as in the one dimensional case except for the grid points at the edges where they do not depend on the next point as it is not next to it. For T_y it is a bit different as seen in figure 4.4. The derivative at point i depends on point $i + N_x$ and $i - N_x$. But the derivative can be calculated in the same way as in equation 4.6 if one just changes the indices such that it is the grid points above and below the point in question that is used. The full Hamiltonian can the be solved by finding the eigenvalues of the sum $H = T_x + T_y + V$. The convergence of this is the same as for the one dimensional case, but the number of points necessary is squared, as the same amount of grid points is required in each dimension. This puts a limit on the size of the systems that can be studied in two dimensions. For example, a system of three particles in one dimension with no center of mass dependence is two dimensional, but with this method studying the weakly bound case of this becomes harder as the solutions fill out most of the grid.

4.2 Integration based methods

When studying the weakly bound states the method of discretizing the Schrödinger equation on a grid and solving for the full spectrum of eigenvalues becomes inefficient. The boundary conditions of the wavefunction being zero at the edges of the box also becomes increasingly inaccurate.

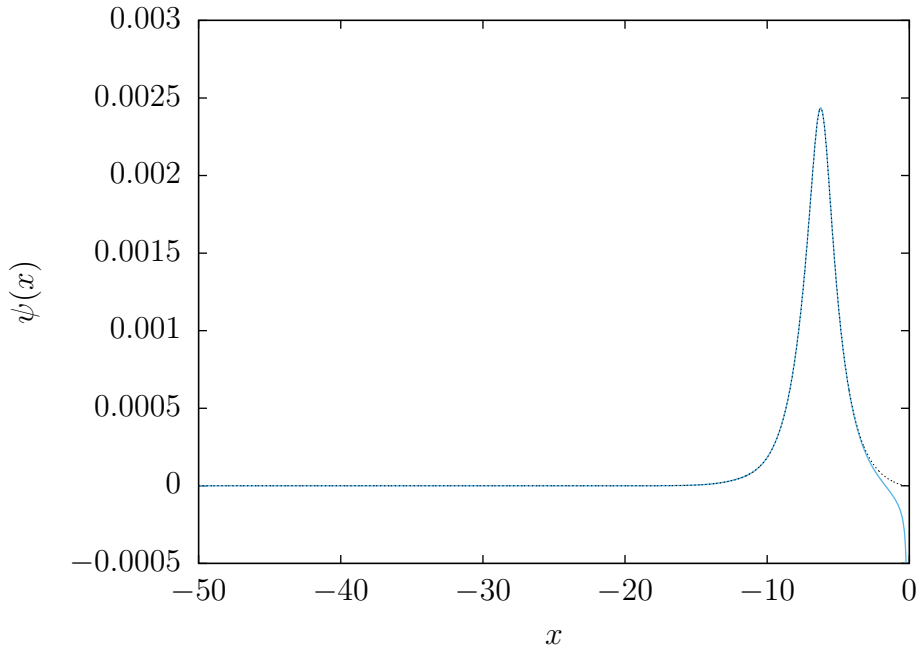

Figure 4.5: Two solutions coming from different initial guesses for the energy. The correct solution goes to zero at $x = 0$ whereas the one with the wrong energy diverges.

For differential equations of the form

$$\left(\frac{d^2}{dx^2} + f(x)\right) y(x) = 0, \tag{4.11}$$

one can calculate the function y(x) if one knows the value at two other points

$$y_{n+1} = \frac{\left(2 - \frac{5h^2}{6} f_n\right) y_n - \left(1 + \frac{h^2}{12} f_{n-1}\right) y_{n-1}}{1 + \frac{h^2}{12} f_{n+1}}, \tag{4.12}$$

where $f_n = f(x_n)$ and $y_n = y(x_n)$ and $h = x_n - x_{n-1}$. Solving the Schrödinger equation with this method we let

$$f(x) = \frac{2\mu}{\hbar^2} \left(E - V(x)\right). \tag{4.13}$$

We start by guessing a value for E, and let $y_0 = \psi(x_0) = exp(-\kappa x_0)$, where $x = 0$ is chosen so $V(x_0) \approx 0$ and we integrate towards $x_n = 0$ and check whether $\psi(0)/\psi'(0) = 0$. If this is not true we repeat the procedure with a different guess for E. In practice this guess is not random and we use a minimization procedure to guess E. In figure 4.5 two functions are shown. The dashed line is the correct energy and one can see how it is 0 at $x = 0$. The full line is for an energy $E = 0.999E_1$, where E_1 is the correct energy. One can see how the two solutions follows each other but the one with the wrong energy diverges at $x = 0$.

Convergence

In this section the convergence of the integration method is calculated as a function of the step size h. In figure 4.6 the lowest eigenvalue is shown as a function of the step size.

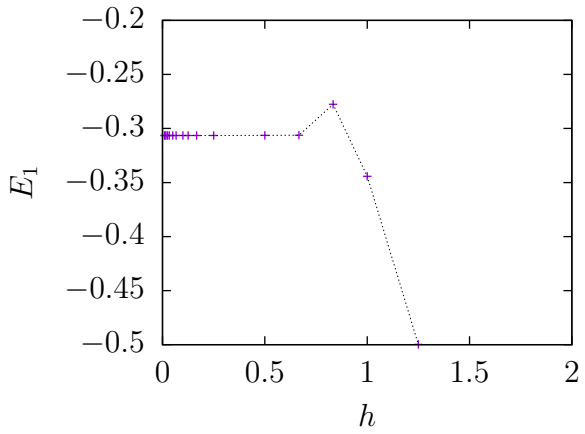

Figure 4.6: The lowest eigenvalue as a function of the step size h this is all calculated by integrating from $x_0 = -50$.

We see that for a step size of $h < 0.5$, the eigenvalue becomes stable. The advantage of this method compared to the grid based method is that with this method we only calculate a single wavefunction, meaning that if we are only interested in the lowest lying states this is much faster than the the grid based method that calculates the full spectrum. This speed advantage makes it possible to go to a larger distance and smaller values of the step size. This makes integration the preferred method to study weakly bound states.

Chapter 5

Quantum single-particle properties in a one-dimensional curved space

In this chapter we leave the world of classical mechanics, and move into the fascinating world of quantum mechanics. We start out by developing a classical description of a single particle moving along a one dimensional wire that is curved through three dimensional space. We then use this classical description to perform a quantization of the motion of the particle, but because of the curved nature of the wire, the ordering of the operators become important. We then take a different approach to the quantization of the motion, and start in three dimensional space, where the normal way of quantizing the motion of a particle is well known. Through an adiabatic approximation, similar to that of the Born-Oppenheimer approximation known from molecular physics, the system is reduced down to a one dimensional system. Finally, we test these different methods of quantizing the same system for three different types of one dimensional geometries.

5.1 Classical Description

We will consider a single particle confined to move in a one dimensional trap. The particle is assumed to be point like with a mass of m_0. Unlike for the particles considered in chapter 3, we only look at a single particle so the only interaction it has is the one that keeps it trapped in one dimension. The geometry of the trap is going to be different variations on the helix shown in chapter 2. In general a one dimensional curve is defined by a parameterization $F : \mathbb{R} \to \mathbb{R}^3$. In this chapter we will use a more general parameterization than the one of the helix used in equation 2.1. It is

$$\{x, y, z\} = R \cdot \{f_x(\phi) \cos\phi, f_y(\phi) \sin\phi, f_z(\phi)\} . \tag{5.1}$$

One can note here that if $f_x = f_y = 1$, and $f_z = \frac{h}{2\pi R}$, then we recover the helix from chapter 2 and 3. Instead of using the full set of three dimensional coordinates to describe the position of the particle we use the parameter ϕ. Because of the more general $f_i(\phi)$ there is no longer an easy interpretation of what the coordinate ϕ describes. We can also calculate the classical velocity $\boldsymbol{v} = \{\dot{x}, \dot{y}, \dot{z}\}$. Where the dots represent the derivative with respect to time. From the velocity one gets the classical kinetic energy T in three dimensions

$$T = \frac{1}{2} m_0 \left(\dot{x}^2 + \dot{y}^2 + \dot{z}^2\right) . \tag{5.2}$$

Through equation 5.1, T can be transformed to only depend on the position on the curve ϕ and the corresponding velocity $\dot{\phi}$. From this the kinetic energy becomes

$$T(\phi, \dot{\phi}) = \frac{1}{2} m_0 (x'^2 + y'^2 + z'^2)\dot{\phi}^2 \equiv \frac{1}{2} m(\phi)\dot{\phi}^2 \ . \tag{5.3}$$

This form of writing the kinetic energy leads to a definition of the effective mass $m(\phi)$. For the type of curves we consider, parameterized through equation 5.1, this leads to an expression for the effective mass

$$\begin{aligned} m(\phi) = m_0 R^2 \big[&(f_x'^2 + f_y^2)\cos^2\phi + (f_x^2 + f_y'^2)\sin^2\phi \\ &+ (f_x f_x' - f_y f_y')\sin(2\phi) + f_z'^2 \big] \ . \end{aligned} \tag{5.4}$$

Here the primes denote derivatives with respect to ϕ, that is $f_y' = \frac{\partial f_y}{\partial \phi}$ etc. A very useful quantity is the conjugate momentum p_ϕ. In classical Lagrangian mechanics it is defined as [35]

$$p_\phi = \frac{\partial T}{\partial \dot{\phi}} = m(\phi)\dot{\phi} \ . \tag{5.5}$$

Inserting the expression for the momentum into the kinetic energy in equation 5.3 we get an expression for the kinetic energy in terms of p_ϕ

$$T = \frac{p_\phi^2}{2m(\phi)} \ . \tag{5.6}$$

The classical kinetic energy of a single particle on a wire will be important when we try to quantize the system in the next section. The position dependent mass in equation 5.4 becomes independent of position if $f_x = f_y$ and f_z' all are independent of ϕ. This is the case for the regular helix where the effective mass is a constant,

$$m(\phi) = m_0 R^2 (f_x^2 + f_z'^2) = m_0 \left(R^2 + \left(\frac{h}{2\pi} \right)^2 \right) . \tag{5.7}$$

If $f_z' = 0$ the helix turns into a circle and the effective mass becomes $m_0 R^2$. We see that is just the mass scaled by the length factor R^2 that shows up because the length is described by the dimensionless variable ϕ. From this we can see that to observe the effect of a position dependent effective mass, it is not enough that the particle follows a curved wire, how the wire curves is equally important.

5.2 Quantizing the motion

When one wants to quantize the motion of a single particle, confined to move in what is effectively a one dimensional trap, there are two distinct approaches on how to do this. The first strategy is to find the classical generalized position and momentum coordinates along the one dimensional trap, and then quantize them in one dimension. How such a quantization should proceed is not always clear, and that will be the topic of this chapter. Another approach without these ambiguous choices in quantization is to start out in three dimensions and then fully quantize the system there. This is a well known technique and has been done since the invention of quantum mechanics. The problem with the second approach is that the system quickly becomes to difficult to solve fully in three dimensions, and then certain approximations are needed to reduce the complexity of the system.

Quantizing in one dimension

For a particle free to move in one dimension the Hamiltonian only contains a kinetic energy term. The traditional way of quantizing the system would then start from equation 5.6 and then introducing the momentum operator $p_\phi = -i\hbar\frac{\partial}{\partial\phi}$. But with a position dependent mass complications arise. p_ϕ and $1/m(\phi)$ no longer commute, and the ordering of the momentum operator and the mass becomes important. The first demand for any particular choice of Hamiltonian is that it is hermitian since all the eigenvalues of the Hamiltonian must be real. A general form of such a Hamiltonian is

$$-\frac{\hbar^2}{2}\frac{1}{m^a}\frac{\partial}{\partial\phi}\frac{1}{m^b}\frac{\partial}{\partial\phi}\frac{1}{m^c}\,, \tag{5.8}$$

from a dimensional analysis we see that the sum $a+b+c=1$ such that the Hamiltonian still has dimension of energy. From the requirement that the Hamiltonian is hermitian we get that $a = c$. This requirement that $a = c$ can be relaxed by introducing an even more general form that is explicitly hermitian

$$-\frac{\hbar^2}{4}\left(\frac{1}{m^a}\frac{\partial}{\partial\phi}\frac{1}{m^b}\frac{\partial}{\partial\phi}\frac{1}{m^c}+\frac{1}{m^c}\frac{\partial}{\partial\phi}\frac{1}{m^b}\frac{\partial}{\partial\phi}\frac{1}{m^a}\right). \tag{5.9}$$

Here we study two particular choices of ordering of the operators namely the case where $a = c = 0$, $b = 1$ and the choice where $a = b = 0$, $c = 1$. These two choices are not arbitrary. The last one $a = b = 0$, $c = 1$ is well known when one want to make a hermitian combination of non-commuting operators. It features when using zero-range interactions at higher orders in for example cold atomic gases, and modern nuclear physics. Both choices show up in nuclear physics, and more exotic things such as quantum gravity research, but also in the topic of quantum guides and apertures. Both choices also show up in the ordering problem of canonical quantization in curved space. It has been argued that to obtain the curved space Hamiltonian that locally is consistent with the JWKB approximation in the semi-classical limit one must take the choice of $a = c = 0$, $b = 1$.

We start out by considering the case where $a = c = 0$ and thus $b = 1$. This choice of effective mass Hamiltonian is one with the mass placed between two momentum operators

$$H_1 = -\frac{\hbar^2}{2}\frac{\partial}{\partial\phi}\frac{1}{m(\phi)}\frac{\partial}{\partial\phi}\,. \tag{5.10}$$

By calculating the derivative of $1/m(\phi)$, and inserting it into the Hamiltonian we can rewrite it in the form

$$H_1 = -\frac{\hbar^2}{2m(\phi)}\frac{\partial^2}{\partial\phi^2}+\frac{\hbar^2 m'(\phi)}{2m^2(\phi)}\frac{\partial}{\partial\phi}. \tag{5.11}$$

This Hamiltonian now has an extra term not only with a derivative of the effective mass but also a first order derivative operator. This is a new feature that is not present in a normal one dimensional Hamiltonian. First order derivatives are usually only something that we see in effective pseudo-potentials. The first order derivative makes it harder to interpret the Hamiltonian, and to compare it with other possible choices. To get rid of it we assume the wavefunction $\Psi(\phi)$ is a product of two functions $\Psi(\phi) = g(\phi)\psi(\phi)$, and

then solve the Schrödinger equation $(H_1 - E)\Psi = 0$ which becommes

$$\begin{aligned}&\frac{-\hbar^2}{2m(\phi)}\Big(g''(\phi)\psi(\phi) + 2g'(\phi)\psi'(\phi) + \psi''(\phi)g(\phi)\Big)\\&+ \frac{\hbar^2 m'(\phi)}{2m^2(\phi)}\Big(g'(\phi)\psi(\phi) + g(\phi)\psi'(\phi)\Big) = Eg(\phi)\psi(\phi).\end{aligned} \tag{5.12}$$

Sorting the terms after what order of $\psi(\phi)$ they include we get the following version of the Schrödinger equation

$$\begin{aligned}&\frac{-\hbar^2}{2m(\phi)}\psi''(\phi)g(\phi) + \hbar^2\psi'(\phi)\left(\frac{m'(\phi)}{2m^2(\phi)} - \frac{g'(\phi)}{m(\phi)}\right)\\&+ \hbar^2\psi(\phi)\left(\frac{g'(\phi)m'(\phi)}{m^2(\phi)} - \frac{g''(\phi)}{2m(\phi)}\right) = Eg(\phi)\psi(\phi).\end{aligned} \tag{5.13}$$

From here we see that the term with the first order derivative in $\psi(\phi)$ disappears if

$$\frac{m'(\phi)}{m^2(\phi)} = 2\frac{g'(\phi)}{g(\phi)}. \tag{5.14}$$

We see here that letting $g(\phi) = m^{1/2}$, that is $\Psi = m^{1/2}\psi$, we get a new Hamiltonian acting on ψ such that $(H_{EM_1} - E)\psi = 0$, this new Hamiltonian is of the form

$$H_{EM_1} = -\frac{\hbar^2}{2m(\phi)}\frac{\partial^2}{\partial\phi^2} + V_{EM_1}, \tag{5.15}$$

Here the first order derivative is gone. We still have a position dependent effective mass and a potential is the price of removing the first order derivative. Adding up all the terms in equation 5.12, we get the potential

$$V_{EM_1} = -\frac{\hbar^2}{4m^2(\phi)}\left(m''(\phi) - \frac{3m'^2(\phi)}{2m(\phi)}\right). \tag{5.16}$$

We now turn to another choice of Hamiltonian with $a = b = 0$ and thus $c = 1$, this is the one where the Hamiltonian is explicitly constructed to be hermitian, with two terms where the ordering of the momentum operators and the effective mass is switched,

$$H_2 = -\frac{\hbar^2}{4}\left(\frac{\partial^2}{\partial\phi^2}\frac{1}{m(\phi)} + \frac{1}{m(\phi)}\frac{\partial^2}{\partial\phi^2}\right). \tag{5.17}$$

Similarly to what we did for H_1 we calculate the derivatives of $1/m(\phi)$. This leads to a Hamiltonian with the same term with a first order derivative as in H_1, but this time there is also a potential term.

$$H_2 = -\frac{\hbar^2}{2m(\phi)}\frac{\partial^2}{\partial\phi^2} + \frac{\hbar^2 m'(\phi)}{2m^2(\phi)}\frac{\partial}{\partial\phi} - \frac{\hbar^2}{4}\frac{\partial^2}{\partial\phi^2}\left(\frac{1}{m(\phi)}\right). \tag{5.18}$$

The first order derivative can be removed by the same trick as used for H_1. Introducing $\Psi = m^{1/2}\psi$. Doing this results in another Hamiltonian H_{EM_2} that acts on ψ in the Schrödinger equation, $(H_{EM_2} - E)\psi = 0$. The only difference between the two Hamiltonians H_{EM_1} and H_{EM_2} is the second order derivative of $1/m(\phi)$. Denoting this difference V_{EM_2} it becomes

$$\begin{aligned}V_{EM_2} &= H_{EM_1} - H_{EM_2}\\&= \frac{\hbar^2}{4}\frac{\partial^2}{\partial\phi^2}\left(\frac{1}{m(\phi)}\right) = \frac{\hbar^2}{4m^2}\big(m'' - 2\frac{m'^2}{m}\big).\end{aligned} \tag{5.19}$$

From this potential we can also see that if the second derivative of $1/m(\phi)$ is zero then $H_{EM_1} = H_{EM_2}$. This is the case if $1/m(\phi) = c_0 + c_1\phi$. This is one of the cases that we will look closer at later. These two choices of Hamiltonian are not the only possible choices, but they represent two different choices that both have shown relevancy in different settings, and we shall later study how their solutions differ on different geometries.

Quantizing in three dimensions

Another approach to quantize the system of a single particle confined to move along a one dimensional trap, is to start from three dimensions. Quantize the system in three dimensions, with the particle in principle free to move in all directions, but then include the confining potential in Hamiltonian

$$H_{3D} = T_x + T_y + T_z + V_{trap}(x, y, z). \tag{5.20}$$

Even for highly symmetric trapping geometries, this quickly turns into a daunting task to solve. Following the approach of [36] where they assume a tight confinement in the directions perpendicular to the trap, and then apply an adiabatic expansion, this leads to only the lowest perpendicular states being excited. But changing curvature along the wire leads to an effective potential

$$H_g = -\frac{\hbar^2}{2m_0}\frac{\partial^2}{\partial s^2} + V_{geo}\ , \tag{5.21}$$

where m_0 is the mass of the particle and it is not position dependent. s is the arclength measured along the curve, and V_{geo} is the geometric potential that is defined as

$$V_{geo} = -\frac{\hbar^2\kappa^2}{8m_0}. \tag{5.22}$$

κ is the curvature of the one dimensional curve, it is a real quantity and thus the geometric potential will always be attractive. The curvature is defined through the Frenet-Serret apparatus [37]. The curvature describes the changes to the tangent vector of a curve. For a curve parameterized as in equation 5.1 the curvature takes the form

$$\kappa^2 = \frac{(z''y' - y''z')^2 + (x''z' - z''x')^2 + (y''x' - x''y')^2}{(x'^2 + y'^2 + z'^2)^3}, \tag{5.23}$$

where the primes denote derivatives with respect to ϕ. The Hamiltonian in equation 5.21 is for a curve parameterized by arc length, whereas the previous Hamiltonians where for curves parameterized by the azimuthal angle, ϕ. To be able to relate the different Hamiltonians we calculate how the arc length s is related to the angle ϕ. The arc length of a curve in $\mathbb{R}^3$ defined by equation 5.1 can be calculated by the following integral:

$$s(\phi) = \int_{\phi_{min}}^{\phi} d\phi\sqrt{x'^2 + y'^2 + z'^2} = \int_{\phi_{min}}^{\phi} \frac{m(\phi)}{m_0}d\phi, \tag{5.24}$$

with this choice we measure from $\phi = \phi_{min}$ and we used the definition of the effective mass from equation 5.3. From this we get that $s' = \sqrt{m(\phi)/m_0}$, this relation can then be used to transform the Hamiltonian in equation 5.21 from the arc length s to the angle ϕ. A direct coordinate transformation, however, is not enough. To make a

proper comparison one have to modify the Hamiltonian and the wave function Ψ_g. The requirement is that the energies calculated from the original Schrödinger equation must be the same as in the modified Schrödinger equation. The modified Hamiltonian H_{geo} then becomes

$$H_{geo} = -\frac{\hbar^2}{2m(\phi)}\frac{\partial^2}{\partial\phi^2} + \frac{\hbar^2 m'(\phi)}{2m^2(\phi)}\frac{\partial}{\partial\phi} + \frac{\hbar^2 m''(\phi)}{8m^2(\phi)} - \frac{7\hbar^2 m'^2(\phi)}{32m^3(\phi)} - \frac{\hbar^2\kappa^2}{8m_0}\,, \tag{5.25}$$

and the corresponding wave function Ψ_{geo} is then

$$\Psi_{geo} = \left(\frac{m(\phi)}{m_0}\right)^{1/4}\Psi_g. \tag{5.26}$$

Both equations 5.25 and 5.26 are now expressed as a function of the ϕ-coordinate. The geometric potential can be rewritten to depend on the effective mass and the derivative of the effective mass. Looking at the expression for the curvature in equation 5.23, one can recognize the denominator as the effective mass cubed. The numerator is more complicated but adding up all the terms we get the following expression for the curvature of the wire

$$\kappa^2 = \frac{\frac{1}{2}mm'' - \frac{1}{4}m'^2 - m(x'x''' + y'y''' + z'z''')}{m^3}\,, \tag{5.27}$$

this can be seen through equations 5.3 and 5.23. From this we see that the curvature can be written as a function of m, m', m'' and further terms containing more than the third derivatives of the parameterization with respect to ϕ.

In the full Hamiltonian with the geometric potential, H_{geo}, the same first order derivative term show up. Similarly as for H_1 and H_2 it can be removed by use of a reduced wave function. We now have three different Hamiltonians describing the same one dimensional system. They are all one dimensional Schrödinger equations, the first two H_{EM_1} and H_{EM_2} only have kinetic energy terms whereas the last one H_{geo} also includes the attractive geometric potential.

Semi-classical approach

With the one dimensional approach being well defined classically, this problems lends itself to a semi-classical approach. This approach gives an alternative to the ambiguous choices of quantization and from them different Hamiltonians. Given appropriate conditions a semi-classical approach can yield valuable insight on a problem. For a semi-classical we turn to the JWKB(Jeffreys-Wentzel-Kramers-Brillouin) approximation[38]. The lowest order bound state solutions take the form

$$\begin{aligned}\Psi_{JWKB}(\phi) = A\cos&\left[\int_{\phi_{min}}^{\phi} d\varphi\sqrt{\frac{2m(\varphi)}{\hbar^2}(E - V(\varphi))}\right] \\ + B\sin&\left[\int_{\phi_{min}}^{\phi} d\varphi\sqrt{\frac{2m(\varphi)}{\hbar^2}(E - V(\varphi))}\right],\end{aligned} \tag{5.28}$$

where again E is the energy of the bound state, and V is the potential along the wire. The integration is over the classically allowed regions that is when $E - V > 0$. The

integrand in the expression is really just the classical momentum from equation 5.5, seeing as $T = E - V$.

The semi-classical approach is only viable if the momentum changes slowly along the wire, normally that means a slowly varying potential. But since the effective mass is also position dependent, too fast variations in the effective mass will also break the applicability of the semi-classical approach.

With no potential along the wire the boundary conditions we use are for the wave functions to be zero at the ends of the wires. This corresponds to infinite potential walls at the ends. With this choice of boundary conditions $\Psi_{JWKB}(\phi_{min}) = 0$ immediately leads to $A = 0$. The condition at the other end, $\Psi_{JWKB}(\phi_{max}) = 0$, leads to the quantization condition

$$\sqrt{\frac{2E_n}{\hbar^2}} \int_{\phi_{min}}^{\phi_{max}} \sqrt{m(\phi)} d\phi = n\pi \ . \tag{5.29}$$

This has a discrete set of solutions E_n, and the corresponding wave functions of the solutions are given by equation 5.28, where $A = 0$. The numerical value of B can then be found by the normalization requirement of $\int_{\phi_{min}}^{\phi_{max}} |\Psi_{JWKB}(\varphi)| d\varphi = 1$. The integral over $\sqrt{m(\phi)}$ is just measuring the length of the wire, and thus the energy spectrum is that of a particle in a infinite square well

$$E_n = \frac{\hbar^2 \pi^2 n^2}{2m_0 L^2(\phi_{max})}, \quad L(\phi) = \int_{\phi_{min}}^{\phi} \sqrt{m(\phi)/m_0} d\phi \ , \tag{5.30}$$

where $L(\phi_{max})$ is just the total length of the wire. This means that the eigenfunctions become

$$\Psi_{JWKB} \propto \sin\left(n\pi L(\phi)/(L(\phi_{max})\right) \ . \tag{5.31}$$

This means that if it is possible to calculate the integral over $\sqrt{m(\phi)}$ analytically, we get an analytical expression for the semi-classical solution which we can compare to the other solutions. One of the systems we consider in the next section, is one where that integral can be solve analytical.

5.3 Solutions in different geometries

In this section we will look at three different variations of the helix. They all correspond to different choices of f_x , f_y and f_z in equation 5.1. We will calculate the lowest lying states of all the different Hamiltonians discussed in the previous section. We saw earlier that a regular helix leads to a constant effective mass, similarly it also leads to a constant curvature. This means that for a regular helix, there is no difference between the different choices of quantization discussed in section 5.2. Even the most general choices of a, b and c in equation 5.9 all lead to the same Hamiltonian. Because of the helix also having a constant curvature, the only difference between the Hamiltonians originating from the one dimension and the one obtained through the adiabatic approximation of the full three dimensional Hamiltonian, is the geometric potential, which for a constant curvature is only a constant shift in the zero point energy. This means that if we want to study the differences between the choices of quantization, we have to add some perturbations to the helix. In the following section we will study three different perturbations.

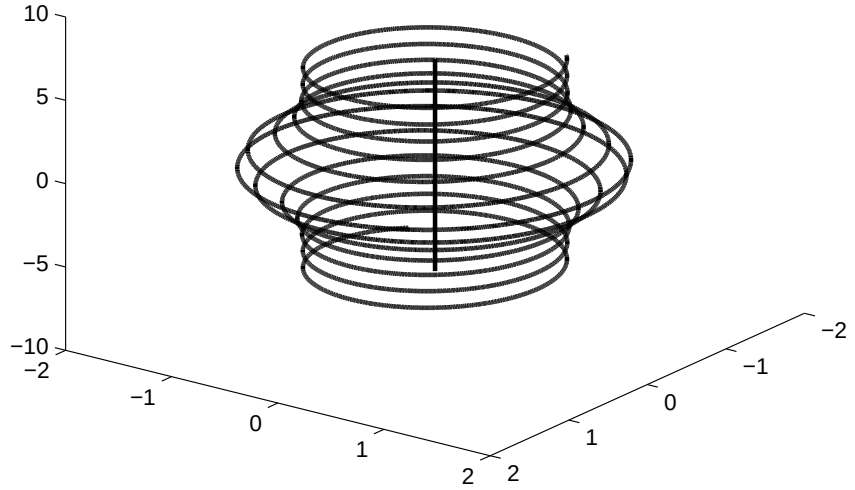

Figure 5.1: A schematic drawing of a helix with a Gaussian deformation of the type in Eq.(5.32). The parameters are chosen to be $a = 0.5$ and $\phi_0 = 4\phi$, and the radius then varies by a factor of 1.5 over about 4 windings. The length can be extended as desired.

The bulging helix

Parameterization

The first of these perturbations that we will study is the bulging helix. This is a helix with varying radius. The pitch of the helix is kept constant while we vary the radius from a constant value at both ends of the helix to a maximum value in the middle. Following equation 5.1 we choose the following parameterization

$$\begin{aligned} f_x(\phi) &= f_y(\phi) = \left(1 + a \cdot \exp(-\phi^2/\phi_0^2)\right) . \\ f_z(\phi) &= \phi \ , \end{aligned} \tag{5.32}$$

here a and ϕ_0 are both positive constants. a is a constant that determines the maximal radius which varies from R to $R(1 + a)$. The increase in the radius follows a Gaussian and ϕ_0 is the width of this Gaussian. We choose to let ϕ run between $\phi_{min} = -40$ and $\phi_{max} = 40$. These values are chosen such that towards the ends of the curve it becomes a regular helix. In figure 5.1 a sketch of how such a perturbation of a helix looks. In this particular case the choice of constants are $a = 0.5$ and $\phi_0 = 2\pi$. This means the radius at the center is 3/2 of that at the ends. The choice of $\phi_0 = 2\pi$, which is one winding of the helix, means that most change in the radius happens within the middle winding.

The position dependence of the effective mass can be calculated from the parameterization in equation 5.32 and the definition of the effective mass in equation 5.4. The expression for the effective mass then becomes

$$m(\phi) = m_0 R^2 \left(1 + \left(\frac{\partial f_x}{\partial \phi}\right)^2 + f_x^2\right) . \tag{5.33}$$

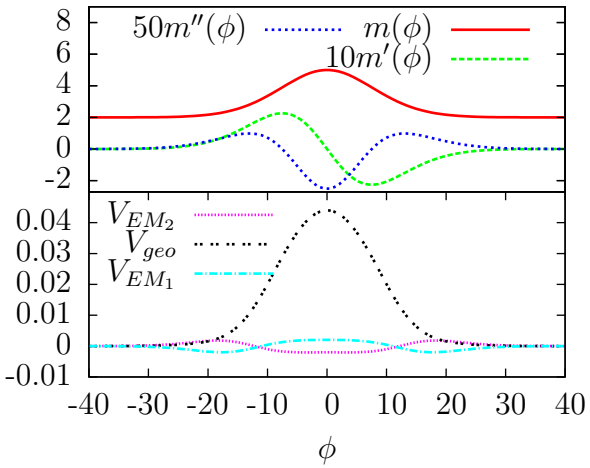

Figure 5.2: Mass and corresponding derivatives as function of angle, ϕ, for the parametrization in Eq.(5.32). Top: $m(\phi)$ (red), $10 \cdot m'(\phi)$ (green), $50 \cdot m''(\phi)$ (blue), all in units of $m_0 R^2$. Bottom contains potentials in units of $\frac{\hbar^2}{4m_0R^2}$ that enter different quantization prescriptions: $V_{EM_1} = -\big(m'' - \frac{3}{2}\frac{m'^2}{m}\big)/m^2$ (dotted, magenta), $V_{EM_2} = \big(m'' - 2\frac{m'^2}{m}\big)/m^2$(dot-dashed, cyan), $V_{geo} = -\kappa^2/2 + V_0$ (dashed, black), see Eqs.(5.15), (5.19) and (5.21). Here $V_0 = 0.1$ is a shift that moves the potential up in order to visualize it along with the other two potentials.

From this all the derivative of the effective mass can be calculated, and from those the different potentials shown in the different choices of Hamiltonians can be calculated as well. In figure 5.2 the dependence of these quantities on ϕ are shown. The top panel in figure 5.2 shows the mass and the first and second order derivative of the mass. The red curve shows the mass which is close to constant in the regions where the radius does not change much, and then it increases at the bulge. The first and second order derivatives are relatively small, they are shown in green and blue respectively. They are both scaled up by a factor to make the variations of them visible on this scale. The relatively small size of the derivatives of the mass implies that the differences between the different quantizations should be small, and at least the solutions should show the same features. The small derivatives of the mass should reflect in the potentials V_{EM_1} and V_{EM_2} that represent the different quantizations. Both potentials are shown in the bottom panel of figure 5.2 and are both small. V_{EM_1} is slightly repulsive at the center, with two attractive regions on either side of the middle before it turns to zero at the ends of the helix. V_{EM_2} shows a similar behavior except with an opposite sign. The geometric potential stemming from the transverse mode adiabatic approximation is shown in black in the bottom panel. With the geometric potential always being negative the curve being shown in figure 5.2 is really $V_{geo} + V_0$, with $V_0 = 0.1$. This was chosen such that it can be seen in the same plot as the other two potentials. We see that V_{geo} is always attractive, but it has a maximum in the center. The scale at which V_{geo} varies, is larger than V_{EM_1} and V_{EM_2}, and we expect it to have a more profound impact on the solutions than the other two potentials.

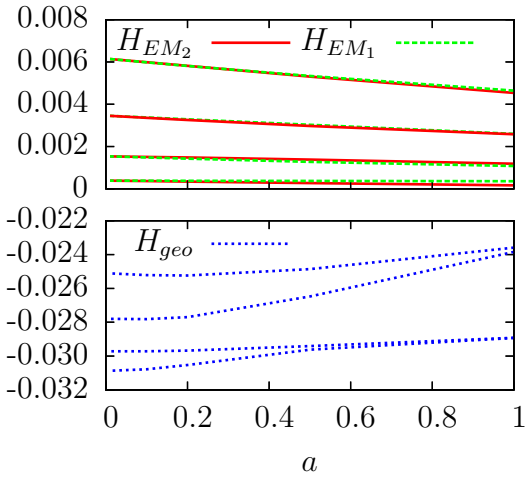

Figure 5.3: The absolute energies of the four lowest states of one particle on a wire parametrized in Eq. (5.32) with $a = 1$ and $\phi_0 = 4\pi$. The energies are in units of $\hbar^2/(R^2 m_0)$. The upper panel shows the energies of H_{EM_1} and H_{EM_2}, whereas the lower one shows the energies of H_{geo}.

Spectra

With the effective mass and all the potentials calculated, we can now solve the different Schrödinger equations. The chosen boundary conditions are that of a particle in a box, i.e the wave function is set to zero at both ends of the wire $\Psi(\phi_{min}) = \Psi(\phi_{max}) = 0$. The Schrödinger equations are solved with the discrete grid based method discussed in chapter 4.

We start out by looking at the spectra of the different Hamiltonians. In tables 5.1 and 5.2, and in figure 5.3, the energies of the four lowest lying states are shown for different values of the parameter a in equation 5.32. In the two tables the ground state energy is the absolute energy of the state where as for the excited states it is the excitation energy that is listed.

Looking at tables 5.1 and 5.2, there is a clear patten in that the energies split up into two groups, those with the geometric potential and those without. The energies of H_{EM_1} and H_{EM_2} are always close, and the energy from the JWKB approximation always falls in between the energies of the two effective mass Hamiltonians. As the energies increase, the differences between the three different solutions becomes smaller, which is in accordance with the move towards the validity of a classical approach. Looking at the JWKB results we see that the energy spectrum shows the expected n^2 scaling known from the infinite square well. From equation 5.30 we expect the energy of the JWKB solutions to scale inversely with the total length of the wire, which can be seen from the constant ratio of 1.160 between all the energies with the different a parameter. The similarities between the three types of solutions without a geometric potential show up already at the lowest energies because of the relatively small variations in the effective mass along the wire.

By including the geometric potential in the Hamiltonians one changes the spectra significantly. With constant curvature towards both ends of the helix and the smaller curvature at the bulge in the center, the geometric potential is always attractive but it is significantly weaker in the middle. This has profound effects on the spectra. The

Table 5.1: The lowest four eigenvalues for different Hamiltonians describing one particle on a wire parametrized in Eq. (5.32) with $a = 1$ and $\phi_0 = 4\pi$. The ground state energies are in absolute values in units of $\hbar^2/(R^2 m_0)$. The excited states are reported as excitation energies related to the corresponding ground state energy.

Hamiltonian	H_{EM_1}	H_{EM_2}	JWKB	H_{geo}	JWKB (including V_{geo})
Ground state	$3.58 \cdot 10^{-4}$	$1.63 \cdot 10^{-4}$	$2.88 \cdot 10^{-4}$	$-2.89 \cdot 10^{-2}$	$-2.76 \cdot 10^{-2}$
1st excited	$7.18 \cdot 10^{-4}$	$1.02 \cdot 10^{-3}$	$8.64 \cdot 10^{-4}$	$8.62 \cdot 10^{-6}$	0
2nd excited	$2.24 \cdot 10^{-3}$	$2.42 \cdot 10^{-3}$	$2.30 \cdot 10^{-3}$	$5.07 \cdot 10^{-3}$	$7.10 \cdot 10^{-3}$
3rd excited	$4.29 \cdot 10^{-3}$	$4.37 \cdot 10^{-3}$	$4.32 \cdot 10^{-3}$	$5.34 \cdot 10^{-3}$	$7.10 \cdot 10^{-3}$

Table 5.2: The same as in table 5.1 for $a = 0.5$ and $\phi_0 = 4\pi$.

Hamiltonian	H_{EM_1}	H_{EM_2}	JWKB	H_{geo}	JWKB (including V_{geo})
Ground state	$3.72 \cdot 10^{-4}$	$2.73 \cdot 10^{-4}$	$3.34 \cdot 10^{-4}$	$-2.96 \cdot 10^{-2}$	$-2.86 \cdot 10^{-2}$
1st excited	$9.01 \cdot 10^{-4}$	$1.10 \cdot 10^{-3}$	$1.00 \cdot 10^{-3}$	$2.07 \cdot 10^{-4}$	0
2nd excited	$2.65 \cdot 10^{-3}$	$2.70 \cdot 10^{-3}$	$2.67 \cdot 10^{-3}$	$3.14 \cdot 10^{-3}$	$1.70 \cdot 10^{-3}$
3rd excited	$4.97 \cdot 10^{-3}$	$5.03 \cdot 10^{-3}$	$5.01 \cdot 10^{-3}$	$4.76 \cdot 10^{-3}$	$3.90 \cdot 10^{-3}$

four lowest states are all negative because of the potential. In figure 5.3 we see how for large a the four states turns into two sets of two-fold degenerate states. This is because with increasing a the bulge increases in size and conversely the curvature at the center decreases. This in turn increases the height of the barrier in the geometric potential and the potential moves toward a two well system. With nothing in the Hamiltonian to introduce a shift between the odd and even parity states, the solutions become degenerate. The degeneracy of the ground state is exact for the JWKB solution that is including the geometric potential, whereas for the exact solution it is only nearly degenerate with an excitation energy of the first excited state that is three orders of magnitude smaller than that of the second excited state. The degeneracy of the JWKB solutions is exact because the wavefunction is set to zero in the classically forbidden region at the center of the helix. A higher order JWKB solution would allow for some tunneling into this region and thus lifting the degeneracy. The introduction of the geometric potential has a much larger influence on the spectrum than the individual variations between H_{EM_1} and H_{EM_2}, both on the ground state energies and on the excitations. In the limit of $a \to 0$, both the effective mass and the curvature becomes constant as we move towards the shape of a regular helix. In this limit the only difference in the spectra of all the Hamiltonians is that the energies of the Hamiltonians with the geometric potential is shifted down by the constant value of the geometric potential compared to the other solutions. This of course is no physical difference as the zero point energy can always be shifted.

Eigenfunctions

To get the full picture of how the different quantizations differ, we also calculate the eigenfunctions of the system. This is done for the same choice of parameters as we used when we calculated the spectra, namely the choice of $a = 0.5$ and $a = 1$ and with the width of the bulge $\phi_0 = 4\pi$.

In figure 5.4 the ground state wavefunctions of the different Hamiltonians are shown. If we start out by looking at the three solutions without the geometric potential, they

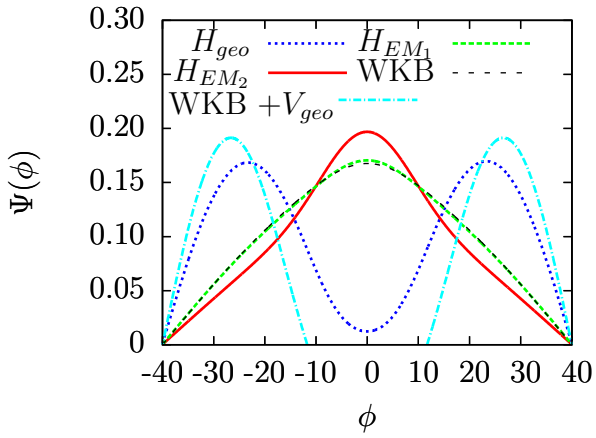

Figure 5.4: Ground state wave functions for the different choices of Hamiltonian, Eq.(5.18) (red), Eq.(5.10) (green), Eq.(5.31) (black), Eq.(5.25) (blue), Eq.(5.28) (light blue). The constants in the parametrization are chosen to be $a = 1$ and $\phi_0 = 4\pi$.

all show the same structure of a single peak at the center of the helix where the bulge is. however the width of the eigenfunction are wider than that of the bulge and the solutions spread out unto the areas that are similar to that of a regular helix. The JWKB solution is almost identical to the solution to H_{EM_1}, whereas the solution to H_{EM_2} is slightly different with a higher peak and a narrower distribution.

The difference between H_{EM_1} and H_{EM_2} is the $\frac{\partial}{\partial\phi}\left(\frac{1}{m(\phi)}\right)$ term shown in figure 5.2. The higher peak is located in the minimum of this potential, and the two upward bends are placed where the potential maxima are located. Introducing the geometric potential greatly changes the picture. The numerical solution to H_{geo} has a minimum at the center, where the other solutions have a maximum. Instead it has two equal maxima on either side of this minimum. This follows from the shape of the geometric potential shown in figure 5.2 where the potential has a maximum right at the center. The JWKB solutions that includes the geometric potential has a similar shape to that of the solution to H_{geo}. But because it is the lowest order JWKB solution it is zero in the classically forbidden region in the center, as mentioned when the spectra was discussed. This could be improved by allowing an exponentially decaying part of the wavefunction in this classically forbidden region.

The first excited states are shown in figure 5.5. They are all calculated for the same parameters as the ground states in figure 5.4. The three solutions without a geometric potential are almost indistinguishable. They all resemble the sine wave function of the first excited state of a square well. The potential minimum at $\phi = 0$ for the extra term in H_{EM_2} is not enough to create a noticeable difference because of the presence of a node at $\phi = 0$.

When the geometric potential is included the eigenfunctions change. The presence of a node at $\phi = 0$ make all the solutions have the same general shape, but the two solution including the geometric potential are pushed further away from the center than the solutions without it. The slope of the two wave functions across the center area with the bulge is much flatter than the other solutions. The JWKB solution that includes the geometric potential is again zero in the classically forbidden region. From the calculation of its spectrum we know that the two states are degenerate. In fact if one takes the

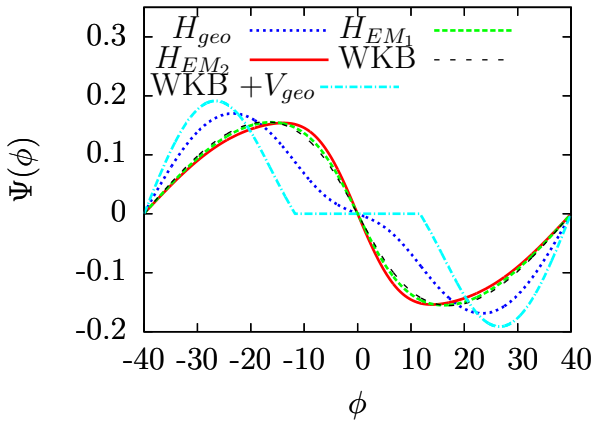

Figure 5.5: First excited states for the different choices of Hamiltonian, Eq.(5.18) (red), Eq.(5.10) (green), Eq.(5.31) (black), Eq.(5.25) (blue), Eq.(5.28) (light blue). The constants in the parametrization are chosen to be $a = 1$ and $\phi_0 = 4\pi$.

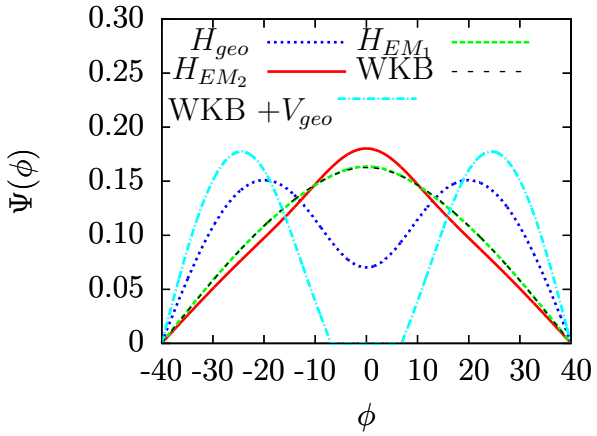

Figure 5.6: Ground states for the different choices of Hamiltonian, Eq.(5.18) (red), Eq.(5.10) (green), Eq.(5.31) (black), Eq.(5.25) (blue), Eq.(5.28) (light blue). The constants in the parametrization are chosen to be $a = 0.5$ and $\phi_0 = 4\pi$.

absolute value of the excited state wave function one would recover the ground state wave function.

In figure 5.6, the ground state wave functions are shown for a different value of the parameter a. The chosen value $a = 0.5$ is half of what it was in the other two figures. The solution to H_{EM_1} and the corresponding JWKB solution has not changed much from figure 5.4, but we see that the solution to H_{EM_2} has moved closer to the other two solutions. Its maximum is lower and the upward bend at the maxima of V_{EM_2} are harder to spot. The two solutions that include the geometric potential are still clearly distinct from the other solutions. The value of the wave function of H_{geo} at its minimum at $\phi = 0$ is more than twice the value of that when $a = 1$. The JWKB solution that includes the geometric potential still has an area around $\phi = 0$ where $E < V(\phi)$, and is thus classically forbidden and the wave function is zero. This is also what one would expect from the dependence of the spectrum on a that we saw in figure 5.3 where the two lowest states of H_{geo} are almost degenerate for $a = 0.5$. If one goes to even smaller

values of a where the two lowest states are clearly separated, then one would expect the JWKB solution to be non-zero along all of the helix.

The stretched helix

The deformations of the helix studied earlier where symmetric around the center of the helix. In the following section we will study two different types of deformation that are not symmetric around the center. They are both variations on the pitch of the helix. Like before we start out by describing the parameterizations and we then calculate the spectra and eigenfunctions of the different quantizations.

Parameterizations

For the first type of deformation we choose a constant stretching of the helix along its rotational axis. The shape in the rotational plane is not changed. This leads to the following parameterization:

$$f_x(\phi) = f_y(\phi) = 1 \ , \ \ f_z(\phi) = a\phi^2 \ , \tag{5.34}$$

where a is a dimensionless constant. The shape in the x-y plane is circular whereas the distance between two neighboring windings increases as ϕ increases. From the parameterization, the effective mass is quickly calculated via equation 5.4. We get

$$m(\phi) = m_0 R^2 \left(1 + 4a^2\phi^2\right) \ . \tag{5.35}$$

One of the advantages of this type of parameterization is that the integral over the square root of the mass in equation 5.29 that defines the quantization in the JWKB solution has an analytical solution. This means that we can get an explicit description of the JWKB wave functions in equation 5.31,

$$\Psi_{JWKB} \propto \sin\left(n\pi L(\phi)/(L(\phi_{max})\right) \ . \tag{5.36}$$

The length is then calculated and becomes

$$\begin{aligned} L(\phi) \quad &= \int_{\phi_{min}}^{\phi} \sqrt{m(\phi)/m_0} d\phi \qquad (5.37) \\ &= R\left(\frac{1}{4a}\ln\left[\frac{\phi + \sqrt{\phi^2 + \frac{1}{4a^2}}}{\phi_{min} + \sqrt{\phi_{min}^2 + \frac{1}{4a^2}}}\right] + a\phi\sqrt{\phi^2 + \frac{1}{4a^2}} - a\phi_{min}\sqrt{\phi_{min}^2 + \frac{1}{4a^2}}\right) \ , \end{aligned}$$

The total length of the wire that is included in equation 5.31 is $L(\phi_{max})$.

The other type of deformation that we will study is inspired by the fact that the two Hamiltonians H_{EM_1} and H_{EM_2} only differ by the second order derivative of the inverse effective mass as seen in equation 5.19. If this term is zero then the difference between the two Hamiltonians vanishes. If we require the parameterization to be circular in the x-y plane, then the effective mass becomes

$$m(\phi) = m_0 R^2 \left(1 + (f_z')^2\right) . \tag{5.38}$$

Then if $1/m(\phi)$ is a first order polynomial or equivalently $m(\phi) = \frac{1}{c_0 + c_1\phi}$, then the term vanishes. we see that for this to be the case $1/(1 + (f_z')^2)$ should be a first order

polynomial. Integrating the requirement for f_z' we get the following parameterization.

$$\begin{aligned} f_x(\phi) &= f_y(\phi) = 1 \\ f_z(\phi) &= -\frac{\arctan\left[\frac{-2c_0-2c_1\phi+1}{2\sqrt{-(c_0+c_1\phi-1)(c_0+c_1\phi)}}\right]}{2c_1} \\ &- \frac{2R\sqrt{-\left(c_0+c_1\phi-1\right)\left(c_0+c_1\phi\right)}}{2c_1}\,, \end{aligned} \tag{5.39}$$

where c_0 and c_1 are dimensionless constants.

The two parameterizations in 5.34 and 5.39 are both monotonous deformations in the z-direction. How they look in three dimensions can be seen in figure 5.7. From the expressions of the mass, their first and second order derivatives can be calculated. The angular dependence of the effective masses and their derivatives are shown in the top panels of figure 5.8 and 5.9. For the parameterization in equation 5.34, we see the expected quadratic behavior of the effective mass, and thus the linear behavior of the derivative of the effective mass. The second order derivative is then a constant with value so small that it cannot be distinguished in the plot.

For the parameterization in equation 5.39 we see how the mass falls of inversely proportional with ϕ, and how the absolute value of both the derivatives falls of with ϕ. Calculating the different combinations of the mass and its derivatives that shows up in H_{EM_1} and H_{EM_2} follows from the previous calculations, and the geometric potential can be calculated for the two parameterizations. All three things are shown in the bottom panels of figure 5.8 and 5.9. For the quadratic stretching of the helix we see in figure 5.8 how the strength of all three potentials quickly falls of with ϕ. V_{EM_1} is attractive for very small ϕ but then it has a barrier at approximately $\phi = 1$, before is quickly falls of from there. V_{EM_2} behaves oppositely by being repulsive for very small ϕ, then having an attractive well at $\phi = 1$, before it also falls of for any values of ϕ larger than that. The geometric potential is always attractive but it also vanishes very quickly. For the parameterization in equation 5.39, V_{EM_1} starts negative before it slowly falls of. The difference between H_{EM_1} and H_{EM_2} is zero by construction where as the geometric potential becomes more and more negative as ϕ increases.

Spectra

We solve the Schrödinger equation for the different quantizations of the two parameterizations in equations 5.34 and 5.39. The boundary conditions are the same as for the bulging helix namely that of a particle in an infinite square well $\Psi(\phi_{min}) = \Psi(\phi_{max}) = 0$. For both parameterization we chose $\phi_{min} = 0$. For the quadratic stretch we have chosen $\phi_{max} = 20$, where as for the squeezed helix we have chosen $\phi_{max} = 40$. The dimensionless parameters that determine the size of the perturbations to the helix have been chosen to be $a = 0.1$, and $c_0 = c_1 = 0.01$. In tables 5.3 and 5.4 the ground state energy and the excitation energies for the first three excited states are shown for the previously mentioned parameters. For both choices of parameterizations there is a clear schism in the energies between the Hamiltonians with a geometric potential and those without.

For the stretched helix the deviations between the energies of H_{EM_1} and the JWKB are largest for the ground states whereas it almost vanishes for the higher excited states. The energies of H_{EM_2} are a bit further off for the ground state. The difference between H_{EM_1} and H_{EM_2} is 42%. For the squeezed helix where $H_{EM_1} = H_{EM_2}$ by construction,

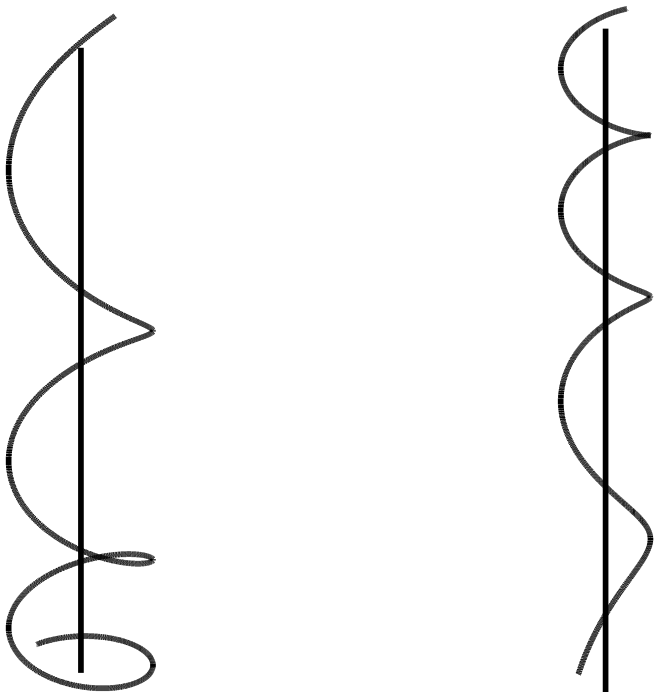

Figure 5.7: Schematic drawings of two deformed helices with stretched and squeezed parameterizations Eqs. (5.35) and (5.39). The stretching and squeezing parameters are chosen to be $a = 0.1$, and $c_0 = c_1 = 0.01$.

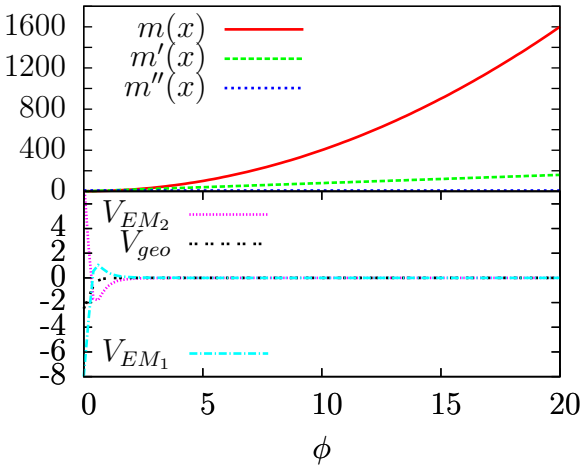

Figure 5.8: Mass and corresponding derivatives as function of angle, ϕ, for the parametrization in eq.(5.34). Top: $m(\phi)$ (red), $m'(\phi)$ (green), $m''(\phi)$ (blue), all in units of m_0R^2. Bottom contains potentials in units of $\frac{\hbar^2}{4m_0R^2}$ that enter different quantization prescriptions: $-\left(m'' - \frac{3}{2}\frac{m'^2}{m}\right)/m^2$(magenta), $\left(m'' - 2\frac{m'^2}{m}\right)/m^2$(cyan), $-\kappa^2/2$(black), see Eqs.(5.15), (5.19) and (5.21).

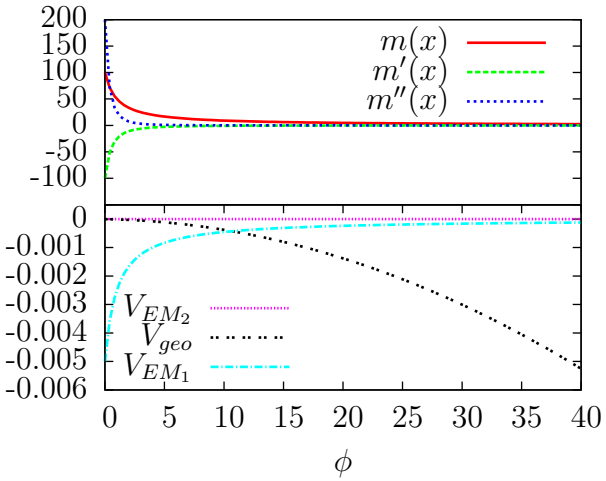

Figure 5.9: Mass and corresponding derivatives as function of angle, ϕ, for the parametrization in eq.(5.39). Top: $m(\phi)$ (red), $m'(\phi)$ (green), $m''(\phi)$ (blue), all in units of m_0R^2. Bottom contains potentials in units of $\frac{\hbar^2}{4m_0R^2}$ that enter different quantization prescriptions: $-\left(m''-\frac{3}{2}\frac{m'^2}{m}\right)/m^2$(magenta), $\left(m''-2\frac{m'^2}{m}\right)/m^2$(cyan), $-\frac{1}{16}\kappa^2/2$(black), see Eqs.(5.15), (5.19) and (5.21).

Table 5.3: The lowest four eigenvalues for different hamiltonians describing one particle on a wire parametrized in Eq. (5.34) with $a = 0.1$ and ϕ varying between $\phi_{min} = 0$ and $\phi_{max} = 20$. The ground state energies are in absolute values in units of $\hbar^2/(R^2m_0)$. The excited states are reported as excitation energies related to the corresponding ground state energy.

Hamiltonian	H_{EM_1}	H_{EM_2}	JWKB	H_{geo}	JWKB (including V_{geo})
Ground state	$2.72 \cdot 10^{-3}$	$1.57 \cdot 10^{-3}$	$2.29 \cdot 10^{-3}$	$-1.51 \cdot 10^{-2}$	$-6.01 \cdot 10^{-3}$
1st excited	$7.00 \cdot 10^{-3}$	$6.59 \cdot 10^{-2}$	$6.85 \cdot 10^{-3}$	$1.69 \cdot 10^{-2}$	$7.46 \cdot 10^{-3}$
2nd excited	$1.84 \cdot 10^{-2}$	$7.72 \cdot 10^{-2}$	$1.84 \cdot 10^{-2}$	$2.63 \cdot 10^{-2}$	$1.70 \cdot 10^{-2}$
3rd excited	$3.43 \cdot 10^{-2}$	$9.31 \cdot 10^{-2}$	$3.44 \cdot 10^{-2}$	$4.11 \cdot 10^{-2}$	$3.19 \cdot 10^{-2}$

Table 5.4: The same as table 5.3 for the parametrization Eq. (5.39) with $c_0 = c_1 = 0.01$ and ϕ varying between $\phi_{min} = 0$ and $\phi_{max} = 40$.

Hamiltonian	H_{EM_1}	H_{EM_2}	JWKB	H_{geo}	JWKB (including V_{geo})
Ground state	$3.93 \cdot 10^{-4}$	$3.93 \cdot 10^{-4}$	$4.22 \cdot 10^{-4}$	$-8.99 \cdot 10^{-3}$	$-6.99 \cdot 10^{-3}$
1st excited	$1.26 \cdot 10^{-3}$	$1.26 \cdot 10^{-3}$	$1.27 \cdot 10^{-3}$	$6.23 \cdot 10^{-3}$	$5.25 \cdot 10^{-3}$
2nd excited	$3.37 \cdot 10^{-3}$	$3.37 \cdot 10^{-3}$	$3.38 \cdot 10^{-3}$	$9.23 \cdot 10^{-3}$	$7.38 \cdot 10^{-3}$
3rd excited	$6.32 \cdot 10^{-3}$	$6.32 \cdot 10^{-3}$	$6.34 \cdot 10^{-3}$	$1.17 \cdot 10^{-2}$	$9.77 \cdot 10^{-3}$

the energies of those two are of course the same, and the energies coming from the JWKB approach are almost the same for the excited states. They are only off by a few percent. Introducing the geometric potential changes things. For the stretched helix the Hamiltonian with the geometric potential holds one bound state and for the squeezed helix it holds two bound states with negative energy. The same is true for the JWKB solutions that include the geometric potential. As for all the other cases, the JWKB solutions approach the full solutions for higher energies.

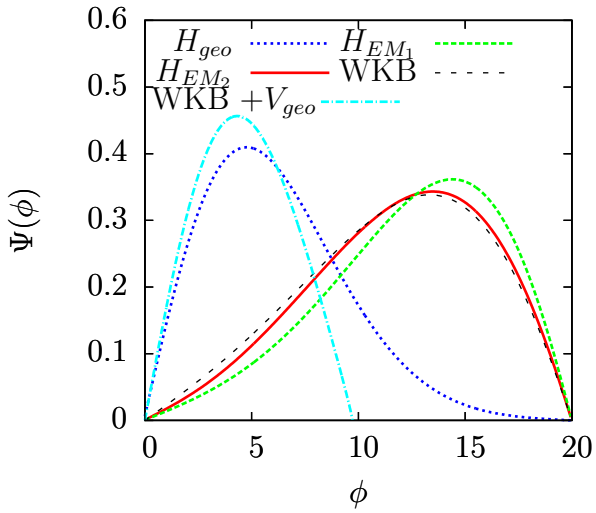

Figure 5.10: Ground states for the different choices of hamiltonian, Eq.(5.18) (red), Eq.((5.10) (green), Eq.(5.25) (blue), Eq.(5.28) (light blue), Eq.(5.31) (black) for the parametrization in Eq.(5.34). The constants in the parametrization are chosen to be $a = 0.1$.

Eigenfunctions of the stretched helix

We now turn to the eigenfunctions of the stretched helix. The parameters are the same as in the previous section, $a = 0.1$, $\phi_{min} = 0$ and $\phi_{max} = 20$. The ground state wave functions are shown in figure 5.10. The solutions to H_{EM_1}, H_{EM_2} and the JWKB solution without the geometric potential all have a single maximum shifted from the middle towards higher values of ϕ. All three wave functions are very similar. The H_{EM_2} and the JWKB solution are hard to distinguish, where as the H_{EM_1} solution has a slightly higher peak shifted towards a higher value of ϕ. The shift of the peak of all three wave functions towards higher values of ϕ is towards the end of the wire where the mass is the highest. The two solutions with the geometric potential are vastly different from the other solutions. They also have a single peak structure but instead of being shifted towards higher values of ϕ they are shifted to a smaller value of ϕ, the peak of both wave functions is narrower than the peaks of the three wave functions without the geometric potential.

The wave functions of the first excited states are shown i figure 5.11. The requirement of a node in all the wave functions diminishes the differences between the two groups of solutions. One can still see the tendency of the solutions without the geometric potential to be at higher values of ϕ and the solutions including the geometric potential to move towards smaller values of ϕ.

Eigenfunctions of the squeezed helix

For the squeezed helix we also calculate the eigenfunctions of the two lowest lying states. The choice of parameters in this case are $\phi_{min} = 0$, $\phi_{max} = 40$ and $c_0 = c_1 = 0.01$. In figure 5.12, the ground state wave functions for all the Hamiltonians are shown. The wave functions here show an opposite behavior from the solutions to the stretched helix. The three solutions without the geometric potential are all shifted towards smaller values of ϕ. The solutions to H_{EM_1} and H_{EM_2} are by construction the same. They have their

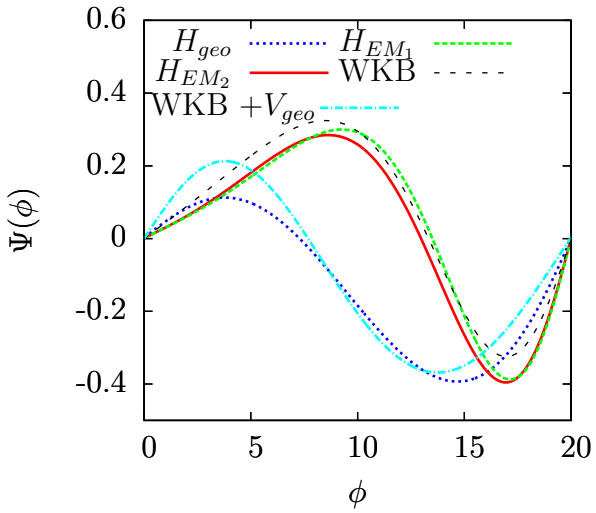

Figure 5.11: Excited states for the different choices of hamiltonian, Eq.(5.18) (red), Eq.(5.10) (green), Eq.(5.25) (blue), Eq.(5.28) (light blue), Eq.(5.31) (black) for the parametrization in Eq.(5.34). The constants in the parametrization are chosen to be $a = 0.1$.

single peak at $\phi = 9$ and from there they fall off almost linearly to 0 at $\phi_{max} = 40$. The JWKB solution has the same features but its maximum is at a slightly higher value of ϕ and the fall off towards ϕ_{max} has a negative curvature compared to the linear nature of the other two. In the same way as for the stretched helix, we see that the two solutions with the geometric potential move to the opposite end of the wire, toward the end with the highest curvature. Both of the wave functions have a narrower peak around $\phi = 32$ and both of them falls of quickly the JWKB solution becomes zero in the classically forbidden region of $\phi < 22$.

The first excited states are shown in figure 5.13. On the figure we see how the three solutions without a geometric potential are drawn toward lower values of ϕ, where as the two that include the geometric potential are at higher values of ϕ. In all the cases, the presence of a node in the first excited state washes out some of the differences between the different Hamiltonians. This is in accordance with how the spectra become more similar at higher energies.

5.4 Summary

We looked at two different approaches to develop a quantum mechanical description of a system of a single particle trapped in an effectively one dimensional trap. The first approach was to start with a classical description of the one dimensional system, and from there develop a quantum mechanical description. But the varying curvature of the trap made the quantization step non-trivial. Among several quantization schemes we considered two particular choices that show up in other areas of physics. The other approach is to start with a fully quantum mechanical description in three dimensions, and then through an adiabatic approximation obtain an effective one dimensional description that includes the so-called geometric potential. This potential is always attractive and is proportional to the square of the curvature of the one dimensional trap. We look at three different perturbations of a helix, and compare the energies and wave functions of

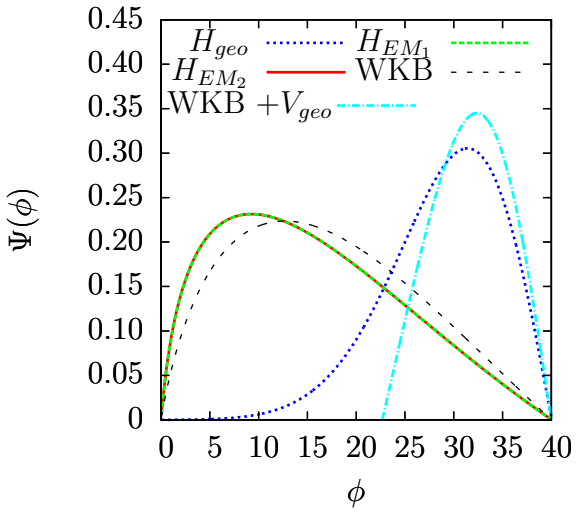

Figure 5.12: Ground states for the different choices of hamiltonian, Eq.(5.18) (red), Eq.((5.10) (green), Eq.(5.25) (blue), Eq.(5.28) (light blue), Eq.(5.31) (black) for the parametrization in Eq.(5.34). The constants in the parametrization are chosen to be $c_0 = 0.01$ and $c_1 = 0.01$.

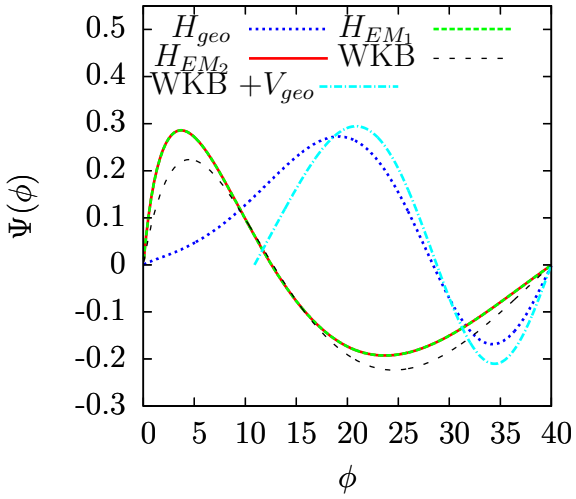

Figure 5.13: First excited states for the different choices of hamiltonian, Eq.(5.18) (red), Eq.((5.10) (green), Eq.(5.25) (blue), Eq.(5.28) (light blue), Eq.(5.31) (black) for the parametrization in Eq.(5.34). The constants in the parametrization are chosen to be $c_0 = 0.01$ and $c_1 = 0.01$.

the three different quantization schemes in each case. We also compare the solutions to the semi classical JWKB solutions. For monotonous deformations of the helix both the effective masses and the curvature becomes monotonous. However, these two properties behave differently. The wave functions that ware solutions to the Hamiltonians with the geometric potential were pulled towards the end with the highest curvature. Whereas the variations of the effective mass meant that the other solutions were pulled in the other direction. This means that these monotonous deformations might lead to observable differences between the different quantization schemes.

Chapter 6

Few-body states of dipoles on a helix

In this chapter we study the bound states of two and three dipoles on a regular helix. The dipoles being on a regular helix implies that all the different quantizations discussed in the previous chapter yield the same result. At most their spectra are shifted by a constant value, which is not relevant to the structure of few-body states.

6.1 One dipole

We place a single dipole of mass m and dipole moment $\boldsymbol{d}$ on a regular helix. In chapter 2, we discussed the features of the regular helix. The regular helix parameterized by the angle ϕ is given by equation 2.1

$$\{x, y, z\} = \left\{ R\sin(\phi), R\cos(\phi), \frac{h\phi}{2\pi} \right\}. \tag{6.1}$$

In this chapter we want to study a quantum mechanical system of one or more dipoles trapped on helix. In chapter 5, we studied single particle states on more general curves. To better relate the regular helix to the work in that chapter we remind that this corresponds to a choice of $f_x = f_y = 1$ and $f_z = \frac{h}{2\pi R}$ in equation 5.1. These choices lead to a position independent effective mass, and thus the mass operator commutes with the momentum operator. This again means the ordering of the different operators does not matter, and H_{EM_1} and H_{EM_2} are the same Hamiltonians. The curvature of a regular helix is also constant. This again means that if one where to compute the geometric potential, then it would be a negative constant of which its only effect would be to change the zero-point of the energy. We can thus freely pick any of the quantizations as they yield the same eigenfunctions for the Hamiltonian of a single particle on a helix:

$$H = \frac{-\hbar^2}{2m\alpha^2}\frac{\partial^2}{\partial\phi^2} \tag{6.2}$$

This Hamiltonians is just like a single particle Hamiltonian of a particle on a straight line except for the $\frac{1}{\alpha^2}$ factor, which show up for the same reason as a factor of $\frac{1}{R^2}$ that shows up for a particle on a circular wire.

6.2 Two dipoles

Introducing a second dipole to the helix means we have to take the dipole-dipole interaction into consideration. Like in chapter 2, we assume that both of the dipoles are aligned along the z-direction by an external field. With the two dipoles placed at positions ϕ_1 and ϕ_2, the two particle Hamiltonian ends up of the form

$$H = \frac{-\hbar^2}{2m\alpha^2}\frac{\partial^2}{\partial\phi_1^2} + \frac{-\hbar^2}{2m\alpha^2}\frac{\partial^2}{\partial\phi_2^2} + V(\phi_1 - \phi_2) \tag{6.3}$$

The two-dipole potential is in equation 2.3 and shown in figure 2.3. The two-dipole potential only depends on the relative angular distance between the dipoles. This suggest that it might be advantageous to perform a change of coordinates to the center of mass $\Phi = \phi_1 + \phi_2$, and the relative coordinate $\phi = \phi_1 - \phi_2$. Doing this transformation the Hamiltonian separates into two Hamiltonians, one for the motion of the center of mass, and one describing the relative motion of the two dipoles:

$$H = H_{cent} + H_{rel} = \frac{-\hbar^2}{2M\alpha^2}\frac{\partial^2}{\partial\Phi^2} + \frac{-\hbar^2}{2\mu\alpha^2}\frac{\partial^2}{\partial\phi^2} + V(\phi), \tag{6.4}$$

where the first term is H_{cent} and the last two terms are H_{rel}. $M = 2m$ is the total mass and $\mu = m/2$ is the reduced mass of the two dipoles. The solutions to the full Hamiltonian will be a product of the solutions to H_{cent} and H_{rel}. The solutions to H_{cent} are plane waves. We will ignore this part of the solution and focus and the solutions to the relative motion. In principle the full solution can always be constructed as a product of the solutions to H_{rel} and the plane wave solutions to H_{cent}.

It is convenient to rewrite the relative Hamiltonian in natural units, $\tilde{H}$. It takes the form

$$\tilde{H} = \frac{-1}{2}\frac{\partial^2}{\partial\phi^2} + \beta\tilde{V}(\phi) \tag{6.5}$$

where β is the potential strength given by

$$\beta = \frac{\mu d^2}{\pi\epsilon_0 R\hbar^2}\left(\frac{\alpha}{R}\right)^2, \tag{6.6}$$

and $\tilde{V}$ is the reduced potential

$$\tilde{V}(\phi) = \frac{1 - cos\phi - \left(\frac{h\phi}{2\pi R}\right)^2}{\left(2\left[1-\cos\phi\right] + \left(\frac{h\phi}{2\pi R}\right)^2\right)^{5/2}} \tag{6.7}$$

The size of the potential strength β now determines which regime we enter, whether it is a strongly bound or a weakly bound regime.

To get a feel for the possible values of β in different experimental setups we first calculate an expression for the numerical value of β, where one just "plugs in" the experimental parameters

$$\beta \approx 0.0149\left[\frac{m}{\mathrm{u}}\right]\left[\frac{d}{\mathrm{Debye}}\right]^2\left[\frac{1\,\mu\mathrm{m}}{R}\right]\left[1 + \left(\frac{h}{2\pi R}\right)^2\right], \tag{6.8}$$

where u is the atomic mass unit. Debye is the unit of the dipole moment and R is measured in micrometers. Let us use the helix parameters from [31], $R \sim 0.56\,\mu$m and

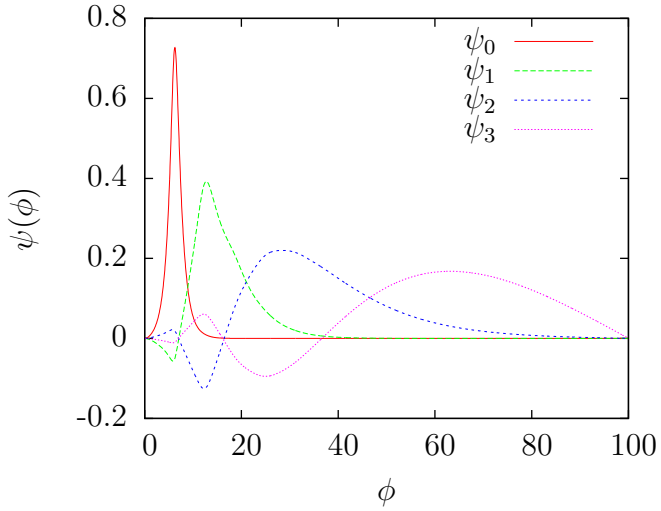

Figure 6.1: The wave functions for four lowest energies with $\beta = 1$. Note how the ground state ψ_0 has its peak at $\phi = \frac{s_{min}}{\alpha}$, the classical equilibrium distance.

$h \sim 1\,\mu$m. We can then insert the parameters from some of the experiments that have managed to create cold heteronuclear molecules with a dipole moment. One example of such molecules is ^{87}Rb-^{133}Cs where a dipole moment of 0.355 Debye has been achieved [39]. Inserting that in equation 6.8 we get $\beta \sim 0.80$. This is a region where the kinetic energy effect are comparable to the interactions. By applying external electric fields, it is possible to tune the dipole moments from zero and up to this maximum value, meaning if one could trap these molecules on a helix one could access both the weak and intermediate interaction regimes with these molecules. There has been other experiments with different polar molecules. In ^{23}Na-^{40}K [40] dipole moments of up to 0.8 Debye has been observed. This would give a value of $\beta \sim 1.6$. For ^{6}Li-^{133}Cs [41, 42] a maximum dipole moment of around 5 Debye has been predicted. This would push to $\beta \sim 100$, meaning that if it is possible to trap some of these heteronuclear molecules on a helix it would be possible to enter both weak and strong interacting regimes.

Solutions to the two-dipole system

We now solve the Schrödinger equation, for the relative motion of the two dipoles. We denote the eigenfunctions $\psi(\phi)$. The one dimensional nature of the this Hamiltonian lends itself to the numerical methods studied in chapter 4. For these first cases we use the grid based method. Similarly to the previous chapter we use the boundary conditions of the particle in a box, i.e the wave function is set to zero at both ends of the helix. Because of the repulsive nature of the short-range dipole-dipole interaction we have $\psi(0) = 0$. With the two dipoles being identical, the symmetry of the relative wave function is determined by whether the dipoles are bosons or fermions. But in both cases it suffices to calculate the wave function only for positive values of the relative coordinate $\phi(\phi_1 > \phi_2)$, and then reconstruct the wave function over both the positive and negative regions of ϕ from the symmetry requirements. Together with the closed boundary conditions, the symmetry requirements means it suffices to solve the Schrödinger equation for a interval $\phi \in [0 : \phi_{max}]$. For this case we have chosen $\phi_{max} = 100$.

For the first case we look at the chosen parameters are $\beta = 1$, and $\frac{h}{R} = 1$. In

figure 6.1, the wave functions for the four lowest lying states are shown. They all have negative energy and are thus bound states of two dipoles. The solid red curve is the ground state. It is tightly located around the classical equilibrium distance of $\phi = 2\pi$. The dashed green curve is the first excited state. It has a small component at the classical equilibrium distance, but because it has to be orthogonal to the ground state most of the wave function is pushed out to the second and third minimum of the potential. The second excited state is the dashed blue curve. The two dipoles are pushed even further apart than for the two lower lying states and the maximum of the wave function is around the fourth or the fifth minimum of the potential. The third excited state is the dashed purple curve. It is pushed out even further than the other three curves. But if one looks at the curvature of the wave function at large ϕ it is negative. since it is positive for the other three, this is a sign of the boundary conditions influencing the wave function. It is the boundary condition at $\phi_{max} = 100$, where the wavefunction is forced to be zero. This is an effect of the chosen numerical method, which is poorly suited for weakly bound states and states that are not bound at all. In the following section we will discuss the size of the bound states and investigate the weakly bound regime where we have to change to another method of solving the Schrödinger equation.

For the choice of $\beta = 1$ the four lowest lying states in figure 6.1 all have negative energy. In figure 6.2, the energy of the four lowest states are shown as a function of β. In this figure we can see that the number of bound states changes as a function of the strength of the potential β. Whether a bound state exists for all possible values of β is in general not possible to answer a priori. In one dimension it is generally true that if the integral over the potential is negative, ie. $\int V(\phi)d\phi \leq 0$, then a bound state exists,[1, 43, 44]. But the two-dipole potential from equation 2.3 diverges at small dipole separations. So to calculate this integral one would need to know the details of the short range forces that appears when two dipoles are brought close to each other. In general this would depend on the types of dipoles chosen, and not just on their dipole moment. This means that the exact value of β where a bound state appears is highly dependent on the short-range physics. It depends on how the system is made, and is out of scope for this thesis, however the general dependence of the number of bound states on the potential strength β is true no matter what type of short-range interactions that come into play.

The size of the bound states

In this section we investigate what happens to the size of the ground state solution when the dipole moment changes. Change in the dipole moment correspond to changes in the dimensionless parameter β. We define the size of a bound state as the expectation value of the squared dipole separation,

$$< \phi^2 >= \int \phi^2 |\psi(\phi)|^2 d\phi. \tag{6.9}$$

For a large dipole strength we expect the system to behave similarly to a harmonic oscillator where the two dipoles are oscillating around the classical equilibrium distance. For a quantum mechanical harmonic oscillator the size of the ground state follows the relation

$$< \phi^2 > \propto \frac{1}{\omega} \propto \frac{1}{\sqrt{\beta}}. \tag{6.10}$$

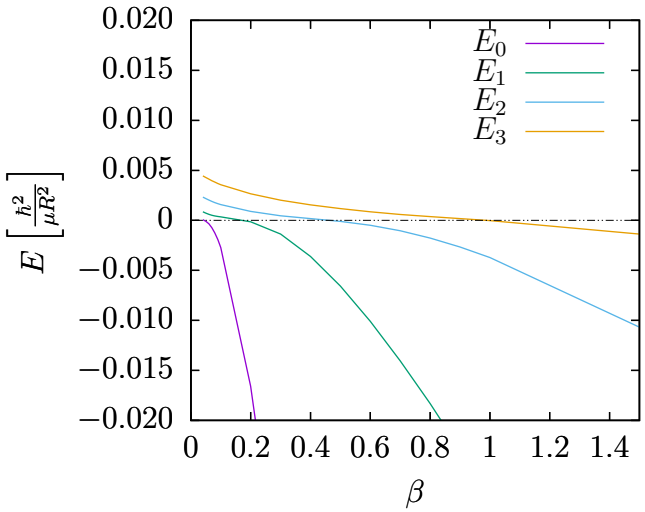

Figure 6.2: The lowest four eigenvalues of two dipoles in a helical trap for different potential strengths β. The energy is in units of $\frac{\hbar^2}{\mu R^2}$.

This is the case for an oscillator centered around zero, but the two dipoles are oscillating at a equilibrium distance of ϕ_0, so we displace the system by ϕ_0 to account for that, i.e.

$$< \phi^2 >= c_1 \frac{1}{\sqrt{\beta}} + c_2 \phi_0^2 \tag{6.11}$$

where c_1 and c_2 are fitting parameters. The specific value of these parameters is not what we are looking for, but rather we want to study whether the size of the ground state scales as equation 6.11. In figure 6.3, the size of the ground state $< \phi^2 >$ is shown as a function of the potential strength β together with a fit to equation 6.11. We see how in the limit of β large the size of the ground state scales as of that of a harmonic oscillator. In the figure we see that for smaller values of β the size of the bound state does not follow this behavior and this leads us to investigate what happens in the other limit of small β.

For small β we expect the system of two dipoles to approach that of free particles, meaning that the wave function asymptotically approaches the form

$$\psi(\phi) = e^{-\kappa\phi}, \tag{6.12}$$

where $\kappa = \sqrt{2E}$. Using this asymptotic form of the wave function we can calculate the size of the wave function as a function of the energy E or the potential strength β. Since the asymptotic form in equation 6.12 is not normalized we calculate the size of the bound state as

$$\langle \phi^2 \rangle = \frac{\int_0^\infty \phi^2 e^{-2\kappa\phi} d\phi}{\int_0^\infty e^{-2\kappa\phi} d\phi} = \frac{1}{2\kappa^2}. \tag{6.13}$$

This means that for low energies, we expect the size of the bound state $< \phi^2 >$ to scale as $\frac{1}{E}$.

When we go to small dipole strength we expect the ground state to asymptotically take the form of equation 6.12. This means that the boundary condition of the wave function at large ϕ is going to be a problem, so for these calculations we use the Numerov method described in chapter 4. In figure 6.4 we show the product of size of the ground

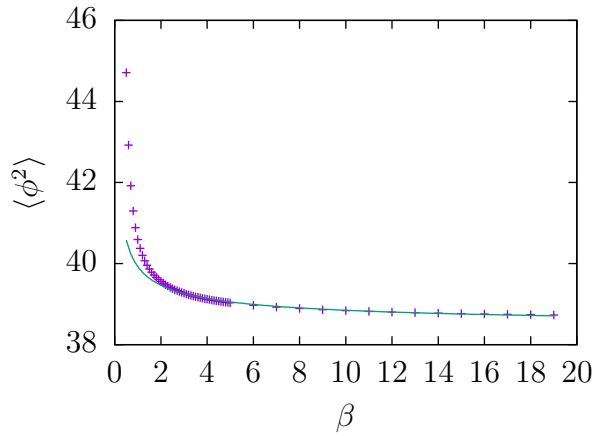

Figure 6.3: The expectation value of ϕ^2 as a function of β with a fit to equation 6.11

state $\langle\phi^2\rangle$ and the ground state energy E as a function of the energy. If equation 6.13 is correct we expect this to approach a constant as the energy approaches zero. The first thing that springs to mind when one looks at figure 6.4 is the clean linear dependence of $\langle\phi^2\rangle|E|$ with increasing $|E|$. This is in clear disagreement with equation 6.13. But we also note that this because the bound state is shifted from 0 to ϕ_0 and the product $(\langle\phi^2\rangle - \phi_0^2)|E|$ is roughly constant over a larger region of $|E|$. This means that we can parameterize the size as $\langle\phi^2\rangle \approx \phi_0^2 + 0.75/|E|$. Unfortunately if equation 6.13 is correct then the constant should have been 0.25. The constant behavior actually continues out to even larger values of $|E|$, into the regions shown in figure 6.3. This connection becomes clearer by looking at the harmonic oscillator where $\langle(\phi-\phi_0)^2\rangle = 1/\omega = 1/2|E|$. This implies that the size then scales with a halo part and an harmonic oscillator part $0.25 + 0.5 = 0.75$. If we take a closer look at the small energy scaling of $\langle\phi^2\rangle|E|$, we refer to the inset in figure 6.4 where we see that in the limit of very small $|E|$ it seems to approach the value 0.25 as predicted by equation 6.13.

6.3 Three dipoles

We now introduce another dipole on the helix. It is of the same mass, m, and dipole moment, d, as the other two dipoles. The position of the three dipoles along the helix are now denoted (ϕ_1, ϕ_2, ϕ_3). The three dipoles interact with each other through the dipole-dipole interaction. The full three-dipole Hamiltonian then becomes

$$H = \frac{-\hbar^2}{2m\alpha^2}\frac{\partial^2}{\partial\phi_1^2} + \frac{-\hbar^2}{2m\alpha^2}\frac{\partial^2}{\partial\phi_2^2} + \frac{-\hbar^2}{2m\alpha^2}\frac{\partial^2}{\partial\phi_3^2} + V(\phi_1-\phi_2) + V(\phi_2-\phi_3) + V(\phi_3-\phi_1) \quad (6.14)$$

This means that the potential part of the Hamiltonian will have three terms stemming from each possible pair of dipoles. With the potential only depending on the relative distances between the dipoles, and no external trapping along the length of the helix, we introduce a new set of Jacobian coordinates that highlights the symmetries of the three dipole system. We define the coordinates $\boldsymbol{r} = (x, y, z)^T$ as $J\boldsymbol{r} = (\phi) = (\phi_1, \phi_2, \phi_3)^T$ [45]

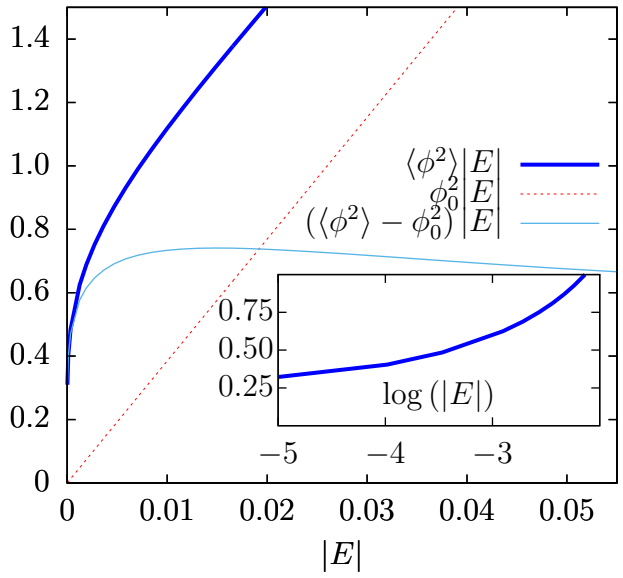

Figure 6.4: The quantities $< \phi^2 > |E|$ (thick blue), $\phi_0^2|E|$ (dashed red), and $(< \phi^2 > -\phi_0^2)|E|$ (thin light blue) as a functions of binding energy for the two-body ground state. The inset is a zoom of $< \phi^2 > |E|$ on the logarithmic scale.

where the transformation is defined as

$$J = \begin{bmatrix} \frac{1}{\sqrt{2}} & \frac{-1}{\sqrt{2}} & 0 \\ \frac{1}{\sqrt{6}} & \frac{1}{\sqrt{6}} & \frac{-\sqrt{2}}{\sqrt{3}} \\ \frac{1}{\sqrt{3}} & \frac{1}{\sqrt{3}} & \frac{1}{\sqrt{3}} \end{bmatrix}. \tag{6.15}$$

This means that the relations between the angles of the dipoles and the new coordinates become

$$\begin{aligned} x &= \frac{1}{\sqrt{2}}\left(\phi_1 - \phi_2\right), \\ y &= \frac{1}{\sqrt{6}}\left(\phi_1 + \phi_2\right) - \sqrt{\frac{2}{3}}\phi_3, \\ z &= \frac{1}{\sqrt{3}}\left(\phi_1 + \phi_2 + \phi_3\right). \end{aligned} \tag{6.16}$$

These coordinates are not the Cartesian coordinates, but rather coordinates measured along the helix. The z coordinate is the center of mass of the full three dipole system. And as for the x and y we shall see that the Hamiltonian separates, thus the system reduces to a two dimensional system in the new x and y coordinates.

To help visualize how the system looks in the xy-space one can see in figure 6.5, how the xy-plane divides into six regions that each corresponds to a different ordering of the three dipoles. This is also useful if one wants to visualize what the different symmetries correspond to. For example, interchanging the position of the first two dipoles ϕ_1 and ϕ_2, from equation 6.16 we see that this corresponds to a change of sign in x meaning a refection about the y-axis in figure 6.5. Similarly a change of $\phi_2 \to \phi_3$ or $\phi_1 \to \phi_3$ results in a reflection about the two diagonals in the figure.

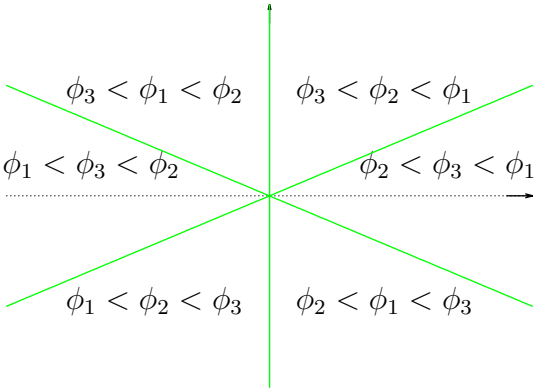

Figure 6.5: Illustration of the xy coordinates in a plane. The green lines correspond to lines across which a pair of particles are exchanged. In each region the ordering of the individual particles is noted.

Performing this coordinate transformation on the full Hamiltonian from equation 6.14 then yields the following relative Hamiltonian in the coordinates x and y

$$H = \frac{-\hbar^2}{2m}\frac{\partial^2}{\partial x^2} + \frac{-\hbar^2}{2m}\frac{\partial^2}{\partial y^2} + V(\sqrt{2}x) + V\left(\sqrt{\frac{3}{2}}y - \frac{1}{\sqrt{2}}x\right) + V\left(\sqrt{\frac{3}{2}}y + \frac{1}{\sqrt{2}}x\right) \quad (6.17)$$

Just like in the case of two dipoles we change to a natural set of units and the Hamiltonian becomes

$$\tilde{H} = -\frac{1}{2}\frac{\partial^2}{\partial x^2} - \frac{1}{2}\frac{\partial^2}{\partial y^2} + \beta\tilde{V}(\sqrt{2}x) + \beta\tilde{V}\left(\sqrt{\frac{3}{2}}y - \frac{1}{\sqrt{2}}x\right) + \beta\tilde{V}\left(\sqrt{\frac{3}{2}}y + \frac{1}{\sqrt{2}}x\right) \quad (6.18)$$

Just like for two dipoles $\tilde{V}$ is the reduced two-dipole potential from equation 6.7, and β is the potential strength from equation 6.6. The units of energy is $\frac{m\alpha^2}{\hbar^2}$. Because the of the repulsive short range part of the two-dipole potential the wave function describing the relative motion of the three dipoles, $\psi(x, y)$ has to be zero when two of the dipoles are at the same position. This corresponds to the three lines in figure 6.5. We can then employ the same trick as for two dipoles, and only solve the problem for one specific ordering of the three dipoles. We choose $\phi_1 > \phi_2 > \phi_3$, this is the upper right area in figure 6.5. Then if the dipoles are either bosons or fermions, we can the use the symmetry requirements to construct the either fully symmetric or antisymmetric wave function for all values of ϕ_1, ϕ_2 and ϕ_3. To solve the two dimensional Schrödinger equation, we discretize the area with $x \in [0 : 160]$ and $y > \frac{1}{\sqrt{3}}x$, following the steps described in chapter 4.

Behavior of the solutions

In figure 6.6 the ground state wave function of three dipoles on helix is shown. It is calculated with a choice of $\beta = 1$ and $\frac{h}{R} = 1$. The surface depicts the value of the wave function and the projection onto the xy-plane is a contour plot of it to help guide the eye. We see that it has a single peak at around $(x, y) \sim (4.4, 7.7)$. If we fix the position of the third dipole at $\phi_3 = 0$, then this translates back to the angular positions of the

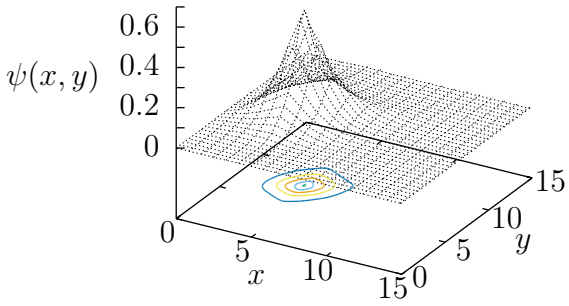

Figure 6.6: The ground state wave function of three dipoles on a helix, with a potential strength $\beta = 1$. The peak is located where the dipoles are sitting one winding apart.

individual dipoles and corresponds to $(\phi_1, \phi_2, \phi_3) = (4\pi, 2\pi, 0)$. This means that the dipoles are situated one winding apart. We saw saw that in the ground state for two dipoles they were sitting one winding apart. Adding a third dipole puts that at the end of the albeit very short chain.

We now turn to the four lowest states of three dipoles on a helix. We show a contour plot of the wave functions in the xy-plane in the four different panels of figure 6.7. Just as for the ground state wave function calculated before, they are all calculated in the area of $y > \frac{1}{\sqrt{3}}x$. However, to make more general structures easier to see we have extended all the wave functions to the positive half plane by assuming all the dipoles are identical bosons. The solid black lines are the symmetry lines also shown in figure 6.5 where $x = \pm\sqrt{3}y$. To get the solutions in the full xy-plane one more reflection across $x = 0$ is need. Do note that the contour plots in figure 6.7 have all been rotated such that the horizontal axis is the y-axis, and the x-axis is vertical. If we had chosen identical fermions instead the wave function would only differ by a sign across the diagonals.

The four panels show the four lowest states of three dipoles on helix with $\beta = 1$ and $\frac{h}{R} = 1$ In the top left panel we see the ground state it is identical to the one shown in figure 6.6. It is three dipoles separated by one winding, the three peaks in the different regions each correspond to a different ordering of the dipoles. The top right panel show the first excited state which has a more elaborate structure. It still has a small peak at the same place as the ground state corresponding to the three dipoles each separated by one winding. But we see that it has two other and larger peaks. These peaks correspond to either the top or the bottom dipole being pushed out to the next winding, corresponding to the second minimum in the two-dipole potential. This behavior is completely analogous to what happened in the two dipole case (figure 6.1), where the first excited state had a small part one winding apart but most of the weight in the second winding.

The second excited state is shown in the lower left panel of figure 6.7. Its structure is not just an easy analogy to the two dipole system. Unlike the two lower lying states,

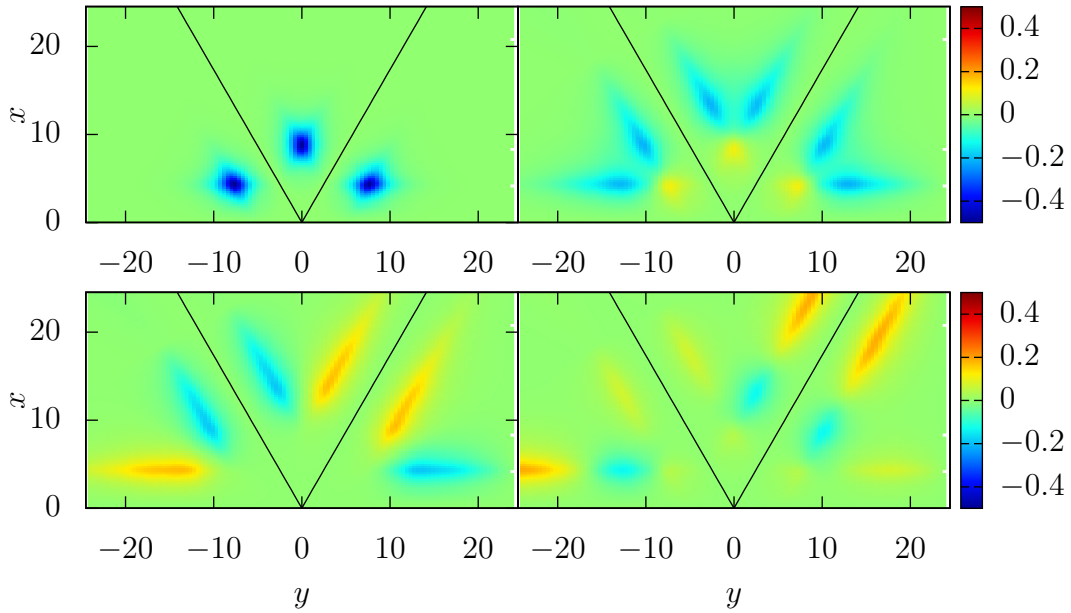

Figure 6.7: The wavefunctions of the four lowest states of 3 dipoles on a helix. (Top left) The ground state. (Top right) The first excited state. (Bottom left) The second excited state. (Bottom right) The third excited state

there is no peak at the position of the three dipoles sitting in a row of three windings. The peaks are much larger in width compared to the other two lower lying states. The structure of these two peaks are very similar to the first excited state the only difference is that they are a bit larger.

The third excited state is shown in the lower right panel of figure 6.7. It follows the trend of the other two excited states. The dipoles are pushed even further apart, seeing as most of the wave function is at even larger values of x and y. It has a small part at the point corresponding to the dipoles sitting in a row. This state, however, is not fully converged. The problem is that the wave function has become too large and it is approaching the boundaries of the box in which it is solved. This problem can be seen by the lack of symmetry within each of the three regions, for the central region it should be symmetric(up to a sign) when $y \to -y$. This operation corresponds to whether it is the top or bottom dipole that is pushed out. This is the same type of effect we saw for the third excited state in the two-dipole system in figure 6.1. We see that even though the third excited state is not well described there is a clear tendency towards the dipoles moving away from the "chain" configuration as we move towards higher excited states, but the ground state configuration is still present in some of the excited states. This just shows the importance of the first minimum in the two dipole potential in equation 6.7 and figure 2.3.

To further investigate the structure of the three dipole system, we look at the relative distance between the dipoles in the ground state. The distance $\phi_{ij} = \phi_i - \phi_j$ are the operators that we are interested in. We calculate the expectation value of these distances in the chosen ordering $\phi_1 > \phi_2 > \phi_3$, where we solved the Schrödinger equation. The results are shown for different values of β for a choice of $\frac{h}{R} = 1$. They are all shown in units of 2π, to show how many windings they are apart. Because of the ordering they are

Table 6.1: The size of the bound states of three dipoles on a helix. This is for a choice of $\beta = 1$ and $h = R$.

β	$\langle\phi_{12}\rangle/2\pi$	$\langle\phi_{23}\rangle/2\pi$	$\langle\phi_{13}\rangle/2\pi$
$\beta = 0.25$	1.50	1.44	2.94
$\beta = 1$	1.01	1.01	2.03
$\beta = 2$	1.00	1.00	2.00

all positive, and they all add up such that $\phi_{13} = \phi_{12} + \phi_{23}$. The calculated expectation values are shown in table 6.1. We see that for larger potential strength, the dipoles tend to form a "chain". We already saw that for the case of $\beta = 1$. For the case of $\beta = 2$ we see that within two decimal places the dipoles are exactly one winding apart. For smaller values of β we expect the dipoles to spread out even further as was the case for two dipoles. For $\beta = 0.25$ we see that the expectation values have increased, and the dipoles are more than winding apart. In this regime the kinetic energy is comparable to the attraction between the dipoles and they are spread out to minimize the kinetic energy and to cover more of the pockets in the potential which we saw in figure 2.3.

Chapter 7

Summary and Outlook

This thesis has studied curved one dimensional geometries, and dipolar particles trapped in them. How to describe the quantum mechanical motion of a single particle in a curved geometry is an interesting topic in its own right. We saw that a non constant curvature leads to a non-trivial quantization step. The interplay between the curved nature of a helix and the long-range dipole-dipole interaction also leads to both some interesting few- and many-body structures.

In chapter 2 the helical trap was introduced. along with the interaction between two dipolar particles trapped in such a helically shaped trap. A first question that is highly relevant for experiments is how for certain helix parameters, h and R, the trap prevents short-range collapse of a system of dipoles as the short-range part of the interaction becomes repulsive. Secondly, the dipole-dipole potential becomes oscillating with several minima corresponding to the dipoles being head-to-tail but one or more windings apart. The depths of these minima fall of as the distance cubed just as the regular three dimensional dipole-dipole interaction.

In chapter 3, crystal structures of dipoles trapped on a helix were discussed. This was discussed from a classical point of view through the total potential energy of all the dipoles trapped on the helix. The stable structures for relatively small densities were a number of chains each consisting of the dipoles almost located head-to-tail in the first minimum for the dipole-dipole potential. The stable structures of chains for h/R larger than 1 was an even distribution of the chains, but for an increasing total number of dipoles on the helix the equidistant configuration became unstable. The new stable states with a lower energy are ones where the chains cluster. The stability of these different chain structures were investigated through calculations of the normal modes. An important finding was that even though the equidistant chain structure became unstable, the new stable clustered structure was still consisting of chains. By increasing the number of chains, and thus the density, the stability of the equidistant configuration was increased seeing as the repulsion between the different chains becomes stronger as the chains are closer. In this chapter, we also studied smaller systems of $N = 12$ and $N = 13$ dipoles. The case of $N = 12$ allowed for symmetric configurations of 2, 3 or 4 chains of dipoles, with a corresponding number of degenerate normal modes. These degeneracies could be lifted by adding an extra dipole and thus breaking the symmetry between the different chains. Another confirmation of the chain picture was how the speed of sound in a crystal of dipoles on a helix does not depend on the number of chains seeing as the sound waves propagate along the chains.

Chapter 5 looked at two different approaches to the system of a single particle trapped in an effective one dimensional trap with a varying curvature. The first approach was to

develop a classical description of the particle in the trap, and then quantize from there, but the varying curvature leads to a position dependent effective mass, and the ordering of the operators in the quantization step becomes important. We showed two equally valid choices for which the Hamiltonians only differed by a potential term. The second approach was to start from a quantum mechanical description in three dimensions, and then through a transverse mode adiabatic approximation reduce the problem to an effective one dimensional system, but this added an extra potential term called the geometric potential. This potential is proportional to the squared curvature of the trap and is always attractive. We looked at three different perturbations of the helically shaped trap. For each perturbations we compared the wave functions and the energies coming from the different quantization schemes, and we compared the results with the solutions from a semi-classical approach. For all three types of perturbations we see that the solutions split up into two groups, those including the geometric potential, and those that do not. Specifically the solutions that include a geometric potential are drawn towards the regions of the trap with the highest curvature whereas the different solutions that do not include a geometric potential are pushed to the other regions of the trap due to by the increased effective mass.

Chapter 6 returned to the study of dipolar particles trapped on a helix. But in this chapter we looked at it from a quantum mechanical point of view. The non-trivial quantization step discussed in 5 is not a problem for a regular helix as the curvature is constant and all the different schemes are equivalent up to a constant shift in all the energies. We studied the formation of two- and three-body bound states. The interaction strength could be described by the dimensionless parameter β, which is the ratio of the dipolar interaction energy to the typical kinetic energy. In the limit of strong interactions both the two and the three dipole states correspond to the dipoles being a single winding apart in the ground state. For weaker interactions the states spread out and the dipoles can no longer be said to be specific number of windings apart. For a moderate strength we see that for three dipoles they form a short chain of the dipoles sitting directly above each other. We also show how the structure of the excited states of three dipoles can be understood in terms of the structure of excited states of two dipoles. Both the case of strong interaction and the case of weak interactions should be within experimental reach. The two and three dipole systems were studied with no external trap along the helix direction. This implies that the center of mass coordinate separated and the systems became one dimensional in the case of two dipoles, and two dimensional in the case of three dipoles. If one wanted to study a case with a trap along the helix direction, then the method used to study the three dipole case would be directly applicable to a two-dipole system with a trapping potential along the helix.

One interesting direction to take this work is to bridge the gap between classical crystal structures discussed in chapter 3 and the chain like behavior of the three dipoles discussed in chapter 6. In one dimension no long range order can exist in the quantum regime, instead one would expect the formation of a Luttinger liquid[46]. This type of system has already been discussed in [47], where they used an harmonic approximation of the dipole-dipole potential. We studied the many-body physics only from a classical energy perspective, but the many-body phases of dipoles on a helix could also be studied by both classical and quantum Monte Carlo[48, 49], or by density-matrix renormalization group method [50]. It is important to note though that the above mentioned work is for purely repulsive interactions, and the system of dipoles on a helix has strong attractive interactions between dipoles on different windings in addition to the repulsive interaction between dipoles in the same winding. This is similar to the bi-layer systems where

dipoles in different layers show pairing but influenced by the repulsive interactions with dipoles in the same layer [51]. Another possibility is that in the strongly interacting case then the attractive nature of the head-to-tail interaction between the different windings, could lead to a sort of 'super'-Tonks state as found on a one dimensional straight line in [52]. In such a case the repulsive part of the interaction might also give rise to a (repulsive) Tonks regime. This would be an interesting competition between different strongly interacting one dimensional states. This we notice is similar to the case of two tubes of dipolar particles seen in [53].

We showed in chapter 6 that for certain interaction strengths the few body states follow that of a harmonic oscillator. Using the harmonic approximation in the strongly interacting limit [54] also makes it possible to study thermodynamic properties of dipolar chains in other geometries [55, 56]. Another interesting direction, is that one of the most promising method of creating a helical trap [31], allows for the creation of a double helix trap, similar to the geometry of DNA chains. If one traps dipoles on both strains one could imagine more involved states, both in the few and many body case. If one traps only a single dipole on each helix then that removes the conditions on $\frac{h}{R}$ that prevents short range collapse of the dipoles seeing as they are now in two different traps. This would be a clean first step to study binding of small complexes in non-trivial geometries. The double helix system is also an interesting system for which to study the many-body phases. This might be done with the same techniques mentioned above. In particular the density-matrix renormalization group method might be a good approach, as one could imagine modeling the double helix like the two-leg ladder implementation in [57]. It might be possible to push this idea even further and look at a triple helix system. There are proposals for studying such systems through the point of view of three-stranded DNA structures [58, 59, 60, 61]. From a few-body point of view one aspect is particularly interesting, namely the possibility of Efimov-like physics in such systems [58], where two strands are only weakly bound, and the three strand system could then show Efimov bound states. It could be interesting to see whether the chain-like structures we found could be used as 'strands'. This could be investigated for the triple helix system, but might also be interesting to investigate whether the quantum behavior for the three chains system on a single helix could form an effective three chain bound system. This would be hard to solve as an N-body system but it might be possible through an effective chain-chain interaction similarly to what has been done for dipoles in a bi-layer system[62].

Bibliography

[1] L.D. Landau and E.M. Lifshits. *Quantum Mechanics: Non-relativistic Theory.* Butterworth Heinemann. Butterworth-Heinemann, 1977.

[2] Immanuel Bloch, Jean Dalibard, and Wilhelm Zwerger. Many-body physics with ultracold gases. *Rev. Mod. Phys.*, 80:885–964, Jul 2008.

[3] M. A. Cazalilla, R. Citro, T. Giamarchi, E. Orignac, and M. Rigol. One dimensional bosons: From condensed matter systems to ultracold gases. *Rev. Mod. Phys.*, 83:1405–1466, Dec 2011.

[4] Xi-Wen Guan, Murray T. Batchelor, and Chaohong Lee. Fermi gases in one dimension: From bethe ansatz to experiments. *Rev. Mod. Phys.*, 85:1633–1691, Nov 2013.

[5] M. Olshanii. Atomic scattering in the presence of an external confinement and a gas of impenetrable bosons. *Phys. Rev. Lett.*, 81:938–941, Aug 1998.

[6] C. J. Pethick and Henrik Smith. *Bose-Einstein condensation in dilute gases.* Cambridge University Press, second ed. edition, 2008.

[7] M. H. Anderson, J. R. Ensher, M. R. Matthews, C. E. Wieman, and E. A. Cornell. Observation of bose-einstein condensation in a dilute atomic vapor. *Science*, 269(5221):198–201, 1995.

[8] Dan M. Stamper-Kurn and Masahito Ueda. Spinor bose gases: Symmetries, magnetism, and quantum dynamics. *Rev. Mod. Phys.*, 85:1191–1244, Jul 2013.

[9] Maciej Lewenstein, Anna Sanpera, Veronica Ahufinger, Bogdan Damski, Aditi Sen(De), and Ujjwal Sen. Ultracold atomic gases in optical lattices: mimicking condensed matter physics and beyond. *Advances in Physics*, 56(2):243–379, 2007.

[10] Tilman Esslinger. Fermi-hubbard physics with atoms in an optical lattice. *Annual Review of Condensed Matter Physics*, 1(1):129–152, 2010.

[11] Cheng Chin, Rudolf Grimm, Paul Julienne, and Eite Tiesinga. Feshbach resonances in ultracold gases. *Rev. Mod. Phys.*, 82:1225–1286, Apr 2010.

[12] S. Inouye, M. R. Andrews, J. Stenger, H.-J. Miesner, D. M. Stamper-Kurn, and W. Ketterle. Observation of feshbach resonances in a bose-einstein condensate. *Nature*, 392(6672):151–154, Mar 1998.

[13] F. Ferlaino and R Grimm. Forty years of efimov physics: How a bizarre prediction turned into a hot topic. *Physics Online Journal*, 3:9, Jan 2010.

[14] V. N. Efimov. Weakly-bound states of three resonantly-interacting particles. *Yad. Fiz*, 12:1080, 1970.

[15] T Lahaye, C Menotti, L Santos, M Lewenstein, and T Pfau. The physics of dipolar bosonic quantum gases. *Reports on Progress in Physics*, 72(12):126401, 2009.

[16] Axel Griesmaier, Jörg Werner, Sven Hensler, Jürgen Stuhler, and Tilman Pfau. Bose-einstein condensation of chromium. *Phys. Rev. Lett.*, 94:160401, Apr 2005.

[17] S. Ospelkaus, A. Pe/'er, K.-K. Ni, J. J. Zirbel, B. Neyenhuis, S. Kotochigova, P. S. Julienne, J. Ye, and D. S. Jin. Efficient state transfer in an ultracold dense gas of heteronuclear molecules. *Nat Phys*, 4(8):622–626, Aug 2008.

[18] K.-K. Ni, S. Ospelkaus, M. H. G. de Miranda, A. Pe'er, B. Neyenhuis, J. J. Zirbel, S. Kotochigova, P. S. Julienne, D. S. Jin, and J. Ye. A high phase-space-density gas of polar molecules. *Science*, 322(5899):231–235, 2008.

[19] J. Deiglmayr, A. Grochola, M. Repp, K. Mörtlbauer, C. Glück, J. Lange, O. Dulieu, R. Wester, and M. Weidemüller. Formation of ultracold polar molecules in the rovibrational ground state. *Phys. Rev. Lett.*, 101:133004, Sep 2008.

[20] F. Lang, K. Winkler, C. Strauss, R. Grimm, and J. Hecker Denschlag. Ultracold triplet molecules in the rovibrational ground state. *Phys. Rev. Lett.*, 101:133005, Sep 2008.

[21] S. Ospelkaus, K.-K. Ni, D. Wang, M. H. G. de Miranda, B. Neyenhuis, G. Quéméner, P. S. Julienne, J. L. Bohn, D. S. Jin, and J. Ye. Quantum-state controlled chemical reactions of ultracold potassium-rubidium molecules. *Science*, 327(5967):853–857, 2010.

[22] K.-K. Ni, S. Ospelkaus, D. Wang, G. Quemener, B. Neyenhuis, M. H. G. de Miranda, J. L. Bohn, J. Ye, and D. S. Jin. Dipolar collisions of polar molecules in the quantum regime. *Nature*, 464(7293):1324–1328, Apr 2010.

[23] E. S. Shuman, J. F. Barry, and D. DeMille. Laser cooling of a diatomic molecule. *Nature*, 467(7317):820–823, Oct 2010.

[24] M. H. G. de Miranda, A. Chotia, B. Neyenhuis, D. Wang, G. Quemener, S. Ospelkaus, J. L. Bohn, J. Ye, and D. S. Jin. Controlling the quantum stereodynamics of ultracold bimolecular reactions. *Nat Phys*, 7(6):502–507, Jun 2011.

[25] Amodsen Chotia, Brian Neyenhuis, Steven A. Moses, Bo Yan, Jacob P. Covey, Michael Foss-Feig, Ana Maria Rey, Deborah S. Jin, and Jun Ye. Long-lived dipolar molecules and feshbach molecules in a 3d optical lattice. *Phys. Rev. Lett.*, 108:080405, Feb 2012.

[26] M. Saffman, T. G. Walker, and K. Mølmer. Quantum information with rydberg atoms. *Rev. Mod. Phys.*, 82:2313–2363, Aug 2010.

[27] A G Volosniev, N T Zinner, D V Fedorov, A S Jensen, and B Wunsch. Bound dimers in bilayers of cold polar molecules. *Journal of Physics B: Atomic, Molecular and Optical Physics*, 44(12):125301, 2011.

[28] A. G. Volosniev, D. V. Fedorov, A. S. Jensen, and N. T. Zinner. Few-body bound-state stability of dipolar molecules in two dimensions. *Phys. Rev. A*, 85:023609, Feb 2012.

[29] M. A. Baranov, M. Dalmonte, G. Pupillo, and P. Zoller. Condensed matter theory of dipolar quantum gases. *Chemical Reviews*, 112(9):5012–5061, 2012. PMID: 22877362.

[30] Aidan S. Arnold. Extending dark optical trapping geometries. *Opt. Lett.*, 37(13):2505–2507, Jul 2012.

[31] Daniel Reitz and Arno Rauschenbeutel. Nanofiber-based double-helix dipole trap for cold neutral atoms. *Optics Communications*, 285(23):4705 – 4708, 2012. Special Issue: Optical micro/nanofibers: Challenges and Opportunities.

[32] John D. Jackson. *Classical Electrodynamics Third Edition*. Wiley, third edition, August 1998.

[33] P. Schmelcher. Effective long-range interactions in confined curved dimensions. *EPL (Europhysics Letters)*, 95(5):50005, 2011.

[34] J K Pedersen, D V Fedorov, A S Jensen, and N T Zinner. Formation of classical crystals of dipolar particles in a helical geometry. *Journal of Physics B: Atomic, Molecular and Optical Physics*, 47(16):165103, 2014.

[35] J.R. Taylor. *Classical Mechanics*. University Science Books, 2005.

[36] J. Stockhofe and P. Schmelcher. Nonadiabatic couplings and gauge-theoretical structure of curved quantum waveguides. *Phys. Rev. A*, 89:033630, Mar 2014.

[37] M.P. do Carmo. *Differential Geometry of Curves and Surfaces*. Prentice-Hall, 1976.

[38] Zelevinsky V. *Quantum Physics*. Wiley, 2010.

[39] Peter K. Molony, Philip D. Gregory, Zhonghua Ji, Bo Lu, Michael P. Köppinger, C. Ruth Le Sueur, Caroline L. Blackley, Jeremy M. Hutson, and Simon L. Cornish. Creation of ultracold $^{87}Rb^{133}Cs$ molecules in the rovibrational ground state. *Phys. Rev. Lett.*, 113:255301, Dec 2014.

[40] Jee Woo Park, Sebastian A. Will, and Martin W. Zwierlein. Ultracold dipolar gas of fermionic $^{23}Na^{40}K$ molecules in their absolute ground state. *Phys. Rev. Lett.*, 114:205302, May 2015.

[41] M. Repp, R. Pires, J. Ulmanis, R. Heck, E. D. Kuhnle, M. Weidemüller, and E. Tiemann. Observation of interspecies ^{6}li-^{133}cs feshbach resonances. *Phys. Rev. A*, 87:010701, Jan 2013.

[42] Shih-Kuang Tung, Colin Parker, Jacob Johansen, Cheng Chin, Yujun Wang, and Paul S. Julienne. Ultracold mixtures of atomic ^{6}li and ^{133}cs with tunable interactions. *Phys. Rev. A*, 87:010702, Jan 2013.

[43] Barry Simon. The bound state of weakly coupled schrödinger operators in one and two dimensions. *Annals of Physics*, 97(2):279 – 288, 1976.

[44] A. G. Volosniev, D. V. Fedorov, A. S. Jensen, and N. T. Zinner. Model independence in two dimensions and polarized cold dipolar molecules. *Phys. Rev. Lett.*, 106:250401, Jun 2011.

[45] N. L. Harshman. Symmetries of three harmonically trapped particles in one dimension. *Phys. Rev. A*, 86:052122, Nov 2012.

[46] Thierry Giamarchi. *Quantum physics in one dimension*. Internat. Ser. Mono. Phys. Clarendon Press, Oxford, 2004.

[47] K. T. Law and D. E. Feldman. Quantum phase transition between a luttinger liquid and a gas of cold molecules. *Phys. Rev. Lett.*, 101:096401, Aug 2008.

[48] G. E. Astrakharchik, Giovanna Morigi, Gabriele De Chiara, and J. Boronat. Ground state of low-dimensional dipolar gases: Linear and zigzag chains. *Phys. Rev. A*, 78:063622, Dec 2008.

[49] G E Astrakharchik, Gabriele De Chiara, Giovanna Morigi, and Jordi Boronat. Thermal and quantum fluctuations in chains of ultracold polar molecules. *Journal of Physics B: Atomic, Molecular and Optical Physics*, 42(15):154026, 2009.

[50] Pietro Silvi, Gabriele De Chiara, Tommaso Calarco, Giovanna Morigi, and Simone Montangero. Full characterization of the quantum linear-zigzag transition in atomic chains. *Annalen der Physik*, 525(10-11):827–832, 2013.

[51] N. T. Zinner, B. Wunsch, D. Pekker, and D.-W. Wang. Bcs-bec crossover in bilayers of cold fermionic polar molecules. *Phys. Rev. A*, 85:013603, Jan 2012.

[52] M. D. Girardeau and G. E. Astrakharchik. Super-tonks-girardeau state in an attractive one-dimensional dipolar gas. *Phys. Rev. Lett.*, 109:235305, Dec 2012.

[53] A G Volosniev, J R Armstrong, D V Fedorov, A S Jensen, M Valiente, and N T Zinner. Bound states of dipolar bosons in one-dimensional systems. *New Journal of Physics*, 15(4):043046, 2013.

[54] J R Armstrong, N T Zinner, D V Fedorov, and A S Jensen. Analytic harmonic approach to the n -body problem. *Journal of Physics B: Atomic, Molecular and Optical Physics*, 44(5):055303, 2011.

[55] Armstrong, J.R., Zinner, N.T., Fedorov, D.V., and Jensen, A.S. Layers of cold dipolar molecules in the harmonic approximation. *Eur. Phys. J. D*, 66(3):85, 2012.

[56] J. R. Armstrong, N. T. Zinner, D. V. Fedorov, and A. S. Jensen. Quantum statistics and thermodynamics in the harmonic approximation. *Phys. Rev. E*, 85:021117, Feb 2012.

[57] Søren Gammelmark and Nikolaj Thomas Zinner. Dipoles on a two-leg ladder. *Phys. Rev. B*, 88:245135, Dec 2013.

[58] Jaya Maji and Somendra M. Bhattacharjee. Efimov effect of triple-stranded dna: Real-space renormalization group and zeros of the partition function. *Phys. Rev. E*, 86:041147, Oct 2012.

[59] Tanmoy Pal, Poulomi Sadhukhan, and Somendra M. Bhattacharjee. Renormalization group limit cycle for three-stranded dna. *Phys. Rev. Lett.*, 110:028105, Jan 2013.

[60] Jaya Maji, Somendra M. Bhattacharjee, Flavio Seno, and Antonio Trovato. Melting behavior and different bound states in three-stranded dna models. *Phys. Rev. E*, 89:012121, Jan 2014.

[61] Tanmoy Pal, Poulomi Sadhukhan, and Somendra M. Bhattacharjee. Efimov-like phase of a three-stranded dna and the renormalization-group limit cycle. *Phys. Rev. E*, 91:042105, Apr 2015.

[62] N.T. Zinner, J.R. Armstrong, A.G. Volosniev, D.V. Fedorov, and A.S. Jensen. Dimers, effective interactions, and pauli blocking effects in a bilayer of cold fermionic polar molecules. *Few-Body Systems*, 53(3-4):369–385, 2012.